Global and Planetary Change 262 (2026) 105467

Contents lists available at ScienceDirect

Global and Planetary Change

journal homepage: www.elsevier.com/locate/gloplacha

Southern component water-driven carbonate dissolution and carbon storage during the Last Glacial Maximum in the western South Atlantic

Jaime Y. Suárez-Ibarra [a,b,*], Bruna B. Dias [c], Sandro M. Petró [d], Cristiane F. Frozza [e,f], Sonia Chaabane [b], Thomas B. Chalk [b], Alexander M. Piotrowski [g], Thibault de Garidel-Thoron [b], Maria A.G. Pivel [h]

[a] Institute of Geology and Palaeontology, Faculty of Science, Charles University, Prague, Czech Republic
[b] Aix-Marseille Université, CNRS, IRD, INRAE, CEREGE, Europôle Méditerranéen de l'Arbois, Aix-en-Provence, France
[c] School of Arts, Sciences and Humanities, Universidade de São Paulo, São Paulo, Brazil
[d] itt OCEANEON – Instituto Tecnológico de Paleoceanografia e Mudanças Climáticas, Universidade do Vale do Rio dos Sinos, São Leopoldo, Brazil
[e] Programa de Pós-Graduação em Geociências, Instituto de Geociências, Universidade Federal do Rio Grande do Sul, Porto Alegre, Brazil
[f] Programa de Pós-Graduação em Geociências, Departamento de Geologia, Universidade Federal de Pernambuco, Recife, Brazil
[g] Department of Earth Sciences, University of Cambridge, Cambridge, United Kingdom
[h] Centro de Estudos de Geologia Costeira e Oceânica (CECO), Instituto de Geociências, Universidade Federal do Rio Grande do Sul, Porto Alegre, Brazil

ARTICLE INFO

Editor: Fabienne Marret-Davies

Keywords:
Water masses geometry
Neodymium isotopes
Productivity
Planktonic foraminifera
Sortable silt
Stable isotopes
Glacial carbon sequestration

ABSTRACT

Late Quaternary glacial-interglacial climate variability is related to the carbon cycle, with its feedback mechanisms amplifying the effects of orbital forcing. These processes account for a ~80–100 ppm change in atmospheric CO_2, and are influenced, in part, by shifts in carbonate production, dissolution, and burial. The southern Brazilian continental margin is close to potential iron fertilisation sources, but the interplay of the region's productivity, water mass geometry, and carbonate dissolution remain underexplored. In this study we investigate core SIS-203 (1894 mbsl depth), covering the 31–7 ka interval. Planktonic foraminifera proxies indicate low productivity during the Last Glacial Maximum (LGM), with a slight increase during the deglaciation and into the Holocene. Authigenic foraminiferal ε_{Nd} shows full influence of corrosive Southern Component Water (SCW) during the LGM, and decreased carbonate preservation supports this interpretation. Thus, despite the low biologically mediated dissolution at this site, carbonate preservation decreases during the LGM, similarly observed in other Atlantic basins. We propose that it is through water mass geometry changes (higher influence of SCW) that calcium carbonate preservation is affected. Changes in deep water mass stratification and circulation strengthened deep-ocean carbon sequestration during the LGM in the western South Atlantic, which may be linked to Southern Hemisphere climate dynamics.

1. Introduction

Late Pleistocene glacial-interglacial cyclicity (Berger, 1988; Milankovitch, 1941) can be observed in global ice volume (as recorded by benthic oxygen-18 isotope [$\delta^{18}O$], Hays et al., 1976; Elderfield et al., 2012), temperature, and atmospheric CO_2 levels (derived from Antarctic ice cores, Bereiter et al., 2015) and exhibits variations paced by orbital cycles. However, the changes introduced by orbital parameters alone cannot fully explain the large observed climatic shifts, invoking the influence of additional feedback mechanisms (Lenton et al., 2008; Shackleton, 2000), such as a tight link to changes in the global marine carbon reservoir (Broecker, 1982; Sigman and Boyle, 2000; Yu et al., 2016). For instance, during the last glacial-interglacial cycles of the late Quaternary, a change in atmospheric CO_2 of approximately 80–100 ppm from glacial to interglacial periods has been documented (Petit et al., 1999), with various feedback mechanisms proposed to explain this amplitude. One proposed mechanism includes a causal chain of events (e.g., Kohfeld and Chase, 2017): the expansion of Antarctic sea ice, which prevents CO_2 degassing and acts to store carbon in the deep ocean by the higher production of nutrient-rich Southern Component Water (SCW) (Railsback et al., 2015; Rickaby et al., 2010). The ice expansion shifts the sea ice edge equatorward and increases the hemispheric heat

* Corresponding author.
E-mail address: suarez@cerege.fr (J.Y. Suárez-Ibarra).

https://doi.org/10.1016/j.gloplacha.2026.105467
Received 29 October 2025; Received in revised form 16 March 2026; Accepted 1 April 2026
Available online 11 April 2026

gradient, strengthening the wind belt (e.g., Kohfeld et al., 2013; Toggweiler et al., 2006), and enhances aeolian iron-bearing dust fertilisation allowing enhanced productivity in the Southern Ocean (e.g., Martin, 1990; Martínez-García et al., 2009). This mechanism is testable in the South Atlantic.

Over the last 25000 years (encompassing Marine Isotope Stages 2 and 1 [MIS 2, MIS 1]), the ocean-climate system underwent significant transformations, including increasing atmospheric CO_2, a marked decrease in global ice volume (last deglaciation, 19–11 ka BP), a southward migration of the southern westerly wind belt, and a decline in biological productivity in the Subantarctic Zone. These changes were particularly pronounced during the transition between the Last Glacial Maximum (LGM, 23–18 ka BP) and Holocene (Clark et al., 2009; Howe et al., 2016a; Kohfeld et al., 2013; Lisiecki and Raymo, 2005; Martínez-García et al., 2009), which in the ocean is marked by a reorganisation of water mass geometries, as well as reduction in both organic carbon and calcium carbonate accumulation rates on regional and global scales (Cartapanis et al., 2016; Mahiques et al., 2007).

The Atlantic Ocean plays an important role in the global thermohaline circulation, transporting salt and heat between hemispheres and is also a critical region to investigate changes in the biological pump which transports carbon from the atmosphere and surface ocean to depth. For instance, in the western South Atlantic, previous studies have also documented a decrease in primary productivity during the last deglaciation (Alvarenga et al., 2022; Frozza et al., 2020; Gu et al., 2017; Pedrão et al., 2022; Pereira et al., 2018; Portilho-Ramos et al., 2019), which likely inhibited carbon export from the mixed layer and sequestration in deep water mass, contributing to net ocean carbon release to the atmosphere. Calcium carbonate preservation responds to changes in the configuration of water masses on regional scales (Liu et al., 2022; Petró et al., 2018a, 2018b; Petró and Burone, 2018; Petró et al., 2021), and also with changes in local primary productivity and organic matter export, however this interplay between water mass configuration and local net export productivity has not been fully explored in the South Atlantic.

Reconstructions based on carbon-13 isotope ($\delta^{13}C$) suggest a pervasive presence of SCW throughout much of the deep South Atlantic during the LGM, implying a major displacement of Northern Component Water (NCW) (Curry and Oppo, 2005; Duplessy et al., 1988) and vertical profiles of benthic $\delta^{13}C$ support greater SCW volume in the Atlantic basin during the LGM than during the Holocene (Shub et al., 2024). However, studies using other proxies point to a sustained production of North Atlantic Deep Water during the LGM, indicating that SCW was less spatially extensive and NCW was more prevalent than the $\delta^{13}C$ data suggests (Blaser et al., 2025; Howe et al., 2016a; Chalk et al., 2019). The extent of NCW relative to SCW at mid- and deep depths of the Atlantic Ocean significantly impacts carbonate preservation, because SCW is less saturated with respect to carbonate ion, reducing the preservation potential of calcium carbonate at the seafloor (Frenz et al., 2003).

Neodymium isotope ratios (ε_{Nd}) is a quasi-conservative tracer for studying water masses (Wu et al., 2022; Yehudai et al., 2023). The isotopic signatures in the ocean are influenced by the age and geological origins of the regions from which the water flows. Sediments on the seafloor acquire coatings of precipitated Fe-and Mn-oxide, and in the case of foraminifera, the coatings contain orders of magnitude more Nd than their shells (Roberts et al., 2012). The oxide coatings incorporate a ε_{Nd} signature corresponding to that of the waters bathing them. As water masses have characteristic ε_{Nd} signatures, the ε_{Nd} of a core site can be interpreted in terms of mixing between water masses. For instance, northern component water (North Atlantic Deep Water) typically shows less radiogenic ε_{Nd} values (ranging from -13 to -10), while southern component water (e.g. Antarctic Bottom Water) displays more radiogenic values (between -8 and -6, Howe et al., 2016b; Pöppelmeier et al., 2022; Robinson et al., 2023; Tachikawa et al., 2017). For these reasons, ε_{Nd} is particularly well-suited to reconstruct Atlantic water mass provenances, and in this study, it is used to trace the relative contributions of northern- and southern-component waters at our core site and thus interrogate the likely impacts of water masses on carbonate preservation.

In this paper, we investigate glacial carbon storage in the deep western South Atlantic during the 31–7 ka interval, focusing on the key processes carbonate dynamics and water mass structure. During the LGM, consistently low biological productivity and the dominant influence of SCW in the region suggest that any intense carbonate dissolution events were driven by short-term changes in water mass geometry toward even less saturated water masses. If so, the deep western South Atlantic may have acted as an important carbon reservoir during the LGM. We test this interpretation with a multi-proxy-approach, based on benthic $\delta^{13}C$, mean sortable silt and ε_{Nd}, documenting signals of dissolution, carbon storage, low flow intensity and water mass provenance.

1.1. Study area

In the Southwest Atlantic, surface circulation is dominated by two oceanographic features: the Subtropical Gyre and the Brazil-Malvinas Confluence. The confluence at ~38°S is the meeting point of the warm (>20°C) and salty (>36 psu) Tropical Water (Fig. 1), that circulate southward in the upper layer forming the Brazil Current. Northward counterflow is formed by the cooler (<15°C), fresher (<34.2 psu) but denser, Subantarctic Water, transported in the upper layer by the Malvinas Current (Peterson and Stramma, 1991; Piola and Matano, 2019).

South Atlantic Central Water circulates near the southern Brazilian continental margin, below the Tropical Water and the Brazil Current. It is cool and nutrient-richer than the overlying water mass (Piola and Matano, 2019) due to the fertilisation of the photic zone from periodic deepwater upwelling events (Lessa et al., 2017, 2019). Below the South Atlantic Central Water, flows SCW encompassing the Antarctic Intermediate Water and Upper Circumpolar Deep Water (UCDW). The NCW exist in a balanced equilibrium with the SCW, flowing southpoleward above a denser SCW, the Antarctic Bottom Water. The presence of SCW promotes dissolution of calcium carbonate due to its undersaturation with respect to carbonate ions, while NCW (North Atlantic Deep Water, NADW) promotes the preservation of calcium carbonate due to its higher carbonate ion concentration (Frenz et al., 2003). Past changes in the proportions of both NCW and SCW have impacted the chemistry of deep water and its carbonate solubility (Curry and Oppo, 2005; Dias et al., 2025; Howe et al., 2018; Howe et al., 2016b; Shub et al., 2024)

2. Material and methods

This study uses sediment samples from piston core SIS-203 (3.6 m length), retrieved from the southern Brazilian continental margin at 1894 meters below sea level (29°30′S, 47°7′W, Fig. 1), currently at the boundary of NADW and UCDW. Core SIS-203 was obtained during an oceanographic campaign during the austral spring-summer of 2007 by *Fugro Brasil* Ltda for the Brazilian National Agency of Petroleum, Natural Gas and Biofuels.

2.1. Foraminiferal analyses

To recover the planktonic foraminifera tests, 38 samples were selected with a mean spacing interval of 9 cm along the core. Each sample was washed through a 63 μm sieve, dried below 60°C and weighed. For the planktonic foraminifera assemblage compositions, at least 300 non-fragmented planktonic foraminifera >150 μm were classified for each sample following the taxonomy of Brummer and Kucera (2022). To reconstruct sea surface primary productivity, we analysed the upwelling-related species *Globigerina bulloides* and the oligotrophic water species *Globigerinoides ruber* (*G.bull/G.rub* ratio) (Conan and Brummer, 2000; Conan et al., 2002), as well as the relative abundance (%) of *Globigerinita glutinata* (Conan and Brummer, 2000; Pereira et al.,

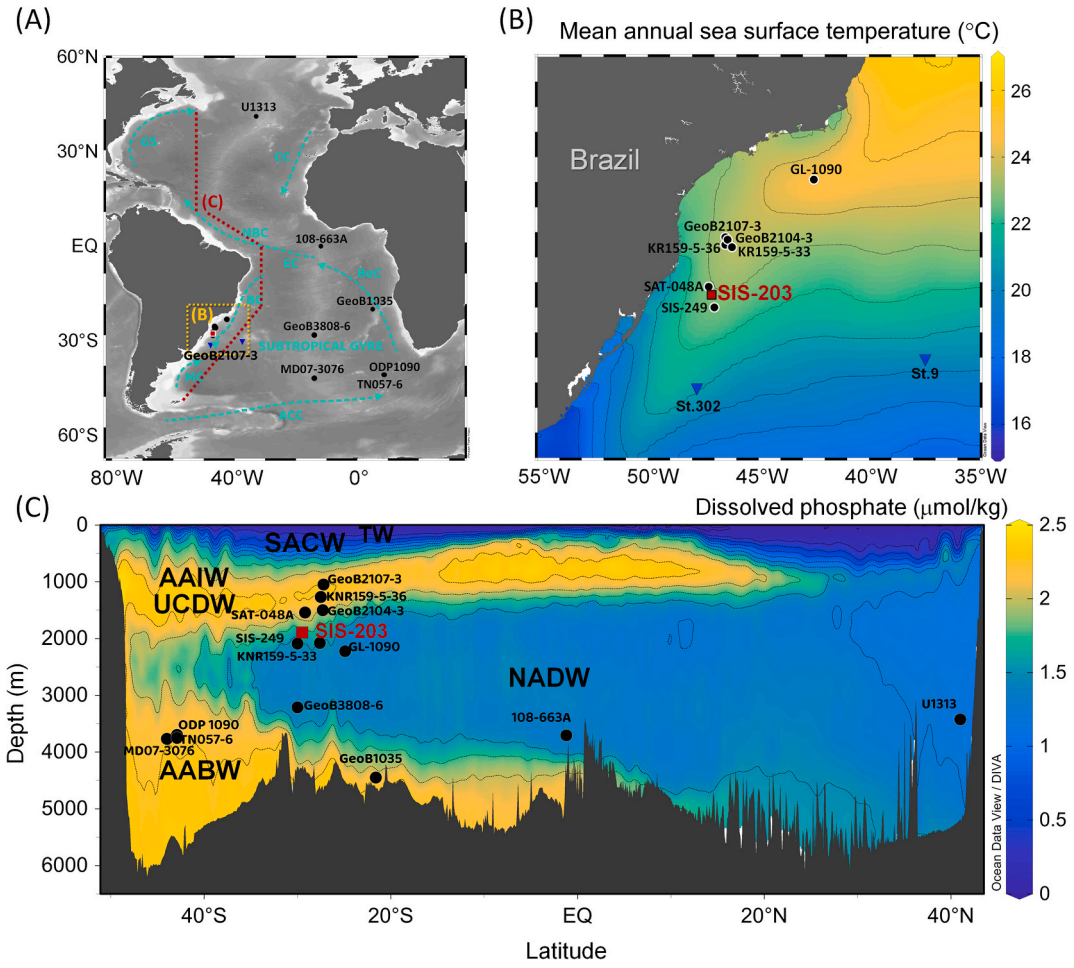

Fig. 1. Location of core SIS-203, other mentioned cores and nearby seawater ε_{Nd} stations. in map view (A), a general overview of the Atlantic surface circulation: BC: Brazil Current; MC: Malvinas Current; ACC: Antarctic Circumpolar Current; BeC: Benguela Current; EC: Equatorial Current; NBC: North Brazil Current; GS: Gulf Stream; CC: Canary Current, (B), detailed map view with mean annual sea surface temperatures (Locarnini et al., 2013) (C) and latitudinal cross section using dissolved phosphate (Garcia et al., 2014) (C). Water masses in C are TW: Tropical Water; SACW: South Atlantic Central Water; AAIW: Antarctic Intermediate Water; UCDW: Upper Circumpolar Deep Water; AABW: Antarctic Bottom Water; (the last three SCW) and NADW: North Atlantic Deep Water (NCW). SIS-203 (this study); U1313 (Chalk et al., 2019); 108-663A (Wagner, 2000); GeoB1035 (Bickert and Wefer, 1996); GeoB3808-6 (Jonkers et al., 2015); ODP1090 (Bickert and Wefer, 1996); TN057-6 (Teitler et al., 2010); MD07-3076 (Skinner et al., 2013); GL-1090 (Howe et al., 2018; Dias et al., 2025); GeoB2107-3 (Howe et al., 2016b); GeoB2104-3 (Howe et al., 2016b); KR159-5-33 (Howe et al., 2018); KR159-5-36 (Howe et al., 2016b); SAT-048A (Suárez-Ibarra et al., 2022); SIS-249 (Suárez-Ibarra et al., 2023); Station (St.) 9 (Wu et al., 2022); St. 302 (Jeandel, 1993). Figure made with Ocean Data View (Schlitzer, 2023).

2018).

To assess calcium carbonate dissolution in core SIS-203, multiple proxies are utilised. The abundance of planktonic foraminifera is presented in terms of individuals per gramme of sediment (Nguyen and Speijer, 2014; Steinsund and Hald, 1994). Parallel, the ratio between the fine (<63 µm) and coarse (>63 µm) sediment fractions was calculated (Berger et al., 1982; Gonzales et al., 2017). Additionally, we used the following dissolution proxy data from core SIS-203, which was published by Petró et al. (2021): benthic *vs.* planktonic foraminifera ratio (the B/P ratio, Kucera, 2007; Parker and Berger, 1971), the calcium carbonate content ($CaCO_3$) (Berger et al., 1982) and planktonic foraminifera fragmentation (Berger, 1970; Le and Shackleton, 1992; Suárez-Ibarra et al., 2021).

2.2. Sedimentological analyses

Calcium carbonate content was measured for 67 samples by measuring the mass-loss after complete reaction with 10% hydrochloric acid (HCl) at the *Centro de Geologia Costeira e Oceânica (CECO)*, *Universidade Federal do Rio Grande do Sul* (UFRGS). Small quantities of HCl solution were added until the reaction was completed. Grain-size analyses of 35 decarbonated (organic matter was not removed) samples were determined using a laser diffraction particle size analyser Horiba Partica-LA-950. Mean sortable silt was calculated as the mean size between the 10–63 µm range within the samples (McCave and Andrews, 2019; McCave and Hall, 2006; McCave et al., 1995). The dry weight of the sediment fractions was determined for 73 samples by sieving the sample into fine (<63 µm) and coarse (>63 µm) fractions. The ratio between respective weights of the fine and coarse fractions, here after referred to as fine/coarse ratio, was calculated.

2.3. Age model

A previous age model was already published for core SIS-203 (Petró et al., 2021). Here we present an improved age model based on six published monospecific Accelerator Mass Spectrometry (AMS) radiocarbon (^{14}C) dates combined with six new oxygen-tie correlation points (Table 1). All AMS radiocarbon ages were measured on planktonic foraminifera *Globigerinoides ruber* (all morphotypes) except at 21 cm, where an additional sample was also analysed on *Globorotalia cultrata*. The AMS radiocarbon ages were calibrated using the IntCal Marine20 curve (Heaton et al., 2020), applying a local reservoir effect (delR) of -85

Table 1
Radiocarbon (^{14}C) ages (from Petró et al., 2021) and oxygen stable isotopes (δ^{18}O) tie-points used for the construction of the age model for core SIS-203 on "*rbacon*" package for R software, listed by increasing depth. Calibration curve (cc) number 2 corresponds to *Marine20* (Heaton et al., 2020). delR and dSTD stand for reservoir effect and reservoir effect error respectively.

Age Control Point Type	Uncalibrated ^{14}C age/δ^{18}O tie-points (years)	Error (years)	Depth (cm)	Calibrated ^{14}C age ranges (at 2σ in years)	cc	delR	dSTD
LAC-UFF170058	6409	27	21	5005–4627	2	-85	40
LAC-UFF170057	7454	31	21	6019–5705	2	-85	40
OxygenTiePoint1	14000	837	39	-	0	0	0
OxygenTiePoint2	17000	837	53	-	0	0	0
LAC-UFF190531	13533	131	58	14051–13225	2	-85	40
LAC-UFF180172	15347	182	124	16335–15371	2	-85	40
LAC-UFF190532	18714	137	199.5	20278–19457	2	-85	40
LAC-UFF190533	19751	157	238.5	21435–20543	2	-85	40
OxygenTiePoint3	25000	837	285	-	0	0	0
OxygenTiePoint4	28000	837	309	-	0	0	0
OxygenTiePoint5	29000	837	332.5	-	0	0	0
OxygenTiePoint6	31500	837	375	-	0	0	0

±40 years, based on Alves et al. (2015); Angulo et al. (2005); Nadal de Masi (1999). For the calculation of the deltaR and calibrated ages, we used the Marine Reservoir Correction Database (http://calib.org/marine/) and the Radiocarbon Calibration Program Calib Rev8.2 (Stuiver and Reimer, 1993).

We correlate the benthic foraminifera (*Uvigerina* spp.) δ^{18}O record (Petró et al., 2021) with the regional benthic δ^{18}O stack for intermediate depths of South Atlantic Ocean (LS16-ISA) (Lisiecki and Stern, 2016). We ran the age model in the R-package "*rbacon*" v. 2.5.3, which implements Bayesian statistics (Blaauw and Christen, 2011). We used an uncertainty of 837 years for the oxygen tie points (Table 1), estimated as the geometric mean of the mean temporal resolution of core SIS-203 (351 years) and the error from the reference curve (~2000 years).

2.4. Stable isotope measurements

Although *Cibicidoides wuellerstorfi* is scarce within the samples, in this study, we analysed 5 samples (3 Holocene and 2 LGM) for δ^{18}O and δ^{13}C, carried out on 4–8 specimens. These samples were analysed at the *Instituto Tecnológico de Paleoceanografia e Mudanças Climáticas* of the *Universidade Do Vale Do Rio Dos Sinos* on a dual inlet isotope ratio mass spectrometer with a Kiel IV carbonate device. Mean error (as 1SD) for these measurements are 0.09 ‰ (δ^{18}O) and 0.06 (δ^{13}C) ‰. A set of δ^{18}O and δ^{13}C analyses were already presented for core SIS-203 (Petró et al., 2021), carried out on 10–15 tests of the more abundant benthic genus *Uvigerina* at the Stable Isotope Laboratory of the University of California, Santa Cruz-CA (SIL-UCSC) on a dual inlet isotope ratio mass spectrometer with a Kiel IV carbonate device. Isotopic data are reported relative to the Vienna Pee-Dee Belemnite (VPDB) standard. 1SD for these data are 0.05 ‰ for δ^{18}O and 0.03 ‰ for δ^{13}C.

2.5. Neodymium isotopes

Authigenic ε_{Nd} analyses were carried out on mixed planktonic foraminifera which have not undergone reductive cleaning to remove their Fe-Mn oxide coatings. Around 60 mg of planktonic foraminifera shells were handpicked from the >150 μm fraction, gently crushed and ultrasonicated to remove clays without removal of the authigenic oxides following Dias et al. (2021, 2025) and Roberts et al. (2012). The cleaned samples were then dissolved in 1 M acetic acid and centrifuged before being transferred to Teflon vials. The supernatants were dried-down before re-dissolution in 0.3 M nitric acid. Rare earth elements (REE) were separated from other elements using Eichrom TRUspec™ resin and neodymium was extracted from the other REE using Eichrom Lnspec™ resin following Larkin et al. (2021). All samples were analysed on a Thermo Neptune Plus multi-collector inductively-coupled plasma mass spectrometer (MC-ICP-MS) at the University of Cambridge (Department of Earth Sciences). Measurements were corrected for mass fractionation to a ^{146}Nd/^{144}Nd ratio of 0.7219. Samples were bracketed with concentration-matched solutions of standard JNdi-1 (Tanaka et al., 2000) with a value of 0.512115±0.000007. Our chronologically youngest (9.5±1.8 ka) ε_{Nd} value is compared with nearby core tops listed in Table 2.

In addition to ε_{Nd} determination, we estimate the relative contributions of NCW (NADW) and SCW (CDW) to the water masses at our study site. For this we use equation (1), which is a mixing model approach from Howe et al. (2016a):

$$\%NCW = \frac{[Nd]_{SCW}\left(\varepsilon_{Nd(NCW)} - \varepsilon_{Nd(SCW)}\right)}{[Nd]_{NCW}\varepsilon_{Nd(NCW)} - [Nd]_{SCW}\varepsilon_{Nd(SCW)} - \varepsilon_{Nd}\varepsilon_{Nd(NCW)} + \varepsilon_{Nd(SCW)}\varepsilon_{Nd}} \times 100 \quad (1)$$

This model considers end-member values for NCW and SCW from published papers (see discussion), and the NCW/SCW proportions were calculated for both Holocene and LGM samples.

2.6. Statistical analyses

We apply principal component analyses (PCA) (Jollife and Cadima, 2016) to synthesise the variation on the palaeoproductivity and carbonate dissolution proxies. We use this approach as all proxies considered here are also thought affected by multiple environmental processes (Suárez-Ibarra et al., 2022; Suárez-Ibarra et al., 2023). The PCA are based on the correlation matrix of the centralised and standardised data. The normalisation is conducted by taking the difference between the dataset mean and the sample value and dividing by the standard deviation of the dataset. The synthesised productivity and dissolution proxies are extracted from the first axes of the PCAs as $PC1_P$ (productivity: *G.bull/G.rub* ratio and *G. glutinata* %) and $PC1_D$ (carbonate

Table 2
Location details of nearby cores compared in this study.

Core	Reference	Depth (mbsl)	Latitude (°)	Longitude (°)
GeoB2107-3	(Howe et al., 2016b)	1050	-27.2	-46.5
KNR159-5-36	(Howe et al., 2016b)	1268	-27.5	-46.5
GeoB2104-3	(Howe et al., 2016b)	1500	-27.3	-46.4
SAT-408A	(Suárez-Ibarra et al., 2022)	1542	-29.1	-47.2
SIS-203	This study	1894	-29.5	-47.1
KNR159-5-33	(Howe et al., 2018)	2082	-27.6	-46.2
SIS-249	(Suárez-Ibarra et al., 2023)	2091	-30.0	-47.0
GL-1090	(Howe et al., 2018)	2225	-24.9	-42.5
GeoB3808-6	(Jonkers et al., 2015)	3213	-30.8	-14.7
MD07-3076	(Skinner et al., 2013)	3770	-44.1	-14.2

dissolution: the B/P ratio, the planktonic foraminifera fragmentation, the $CaCO_3$ %, PF/g and fine/coarse ratio) and following Pearson correlations were both conducted using the software PAST (Hammer et al., 2001), version 4.05.

3. Results

According to our age model, samples from core SIS-203 belong to the 31 to 7 ka BP interval and correspond to the latest Pleistocene and early/middle Holocene (Fig. 2). The *G.bull/G.rub* ratio ranges from 0.04 (at 19 ka BP) to 0.88 (at 28 ka BP) and has a mean value of 0.26±0.17 (Fig. 3). The relative abundance of *G. glutinata* (%, Fig. 3) varies between 7.3 (at 19 ka BP) and 20.2% (at 28 ka BP), with a mean of 12.5±3%. The number of planktonic foraminifera shells per gramme (Fig. 3) varies between 61 (at 17 ka BP) and 1960 (at 7 ka BP) (mean 400). The fine to coarse fraction ratio (<63 μm/>63 μm) ranges between 9 (at 7 ka BP) and 108 (at 17 ka BP), with a mean value of 36.7 (Fig. 3). Mean sortable silt ranged from 25 μm (at 19 ka BP) to 34 μm (at 29 ka BP), with a mean value of 29.6±1.9 μm

The new *Cibicidoides wuellerstorfi* $\delta^{18}O$ ($\delta^{18}O_{Cib}$) and $\delta^{13}C$ ($\delta^{13}C_{Cib}$) analyses from core SIS-203 are shown in Table 3 and Fig. 3. The maximum $\delta^{18}O_{Cib}$ value (4.48 ‰) is recorded at 18.47 ka while the minimum (2.72 ‰) at 8.33 ka BP, consistent with LGM and early Holocene values elsewhere. On the other hand, LGM and early Holocene $\delta^{13}C_{Cib}$ values do not vary significantly (see Table 3).

The ε_{Nd} values range from -7.6 (at 18.4 ka BP) to -9.6 (9.5 ka BP), decreasing from 28.1 to 18.4 ka BP and then increasing towards the core top. The ε_{Nd} mean value is -8.66 ± 0.5 and the analytical error varied between ±0.23 and ±0.4 ε-units (mean 0.33±0.08) (Fig. 3). Furthermore, both PCA analyses yielded first principal components synthesising 65.1% and 67.8% of the variance on the first component for palaeoproductivity and dissolution proxies respectively (Table 4). The cumulative variance reached 100% at PC2 for the productivity proxies and 98.3% (cumulative eigenvalue = 4.90) at PC4 for the dissolution proxies, confirming that the extracted components capture the dominant structure of each dataset. Accumulation rates were generally higher during 31–16 ka BP, between 15–23 cm/kyr, and then decreased during MIS 1 to around 3 cm/kyr (Fig. 3).

4. Discussion

4.1. Age model

The core top ages between our age model and the previously published age model by (Petró et al., 2021) are within uncertainty. However, the base of core SIS-203 exhibits a 30 kyr difference. The age agreement at the top of the core in both models is due to the calibration based on the same ^{14}C dates on planktonic foraminifera (Anderson et al., 1947; Hua, 2009) (Table 1). The disagreement between the age models at the base of the core can be attributed to the fact that Petró et al. (2021) employed AnalySeries (Paillard et al., 1996) to compute the age model, which utilises a linear interpolation scheme: a deterministic approach that heavily relies on tie points. This method produces less reliable models if these points are inaccurately placed, with no capacity for memory to detect outliers, thus, the extremes of the record are subject to erroneous extrapolation. On the other hand, we utilised *rbacon* (Blaauw and Christen, 2011), a Bayesian method that accounts for variability in sediment accumulation rates. The Bayesian model's adherence to realistic accumulation rates suggests a more geologically plausible scenario and rejected the oxygen tie points suggested by Petró et al. (2021) for the base of the core. It seems that the previous age model, based on extrapolation from the final tie point likely maintained unrealistic slowdown in sedimentation rates, placing the base of the core at 60 ka BP, instead of ~30 ka BP.

4.2. Carbonate production and preservation: surface productivity and sinking flux

Calcium carbonate preservation can be affected by early diagenetic processes such as early dissolution due to organic matter degradation in

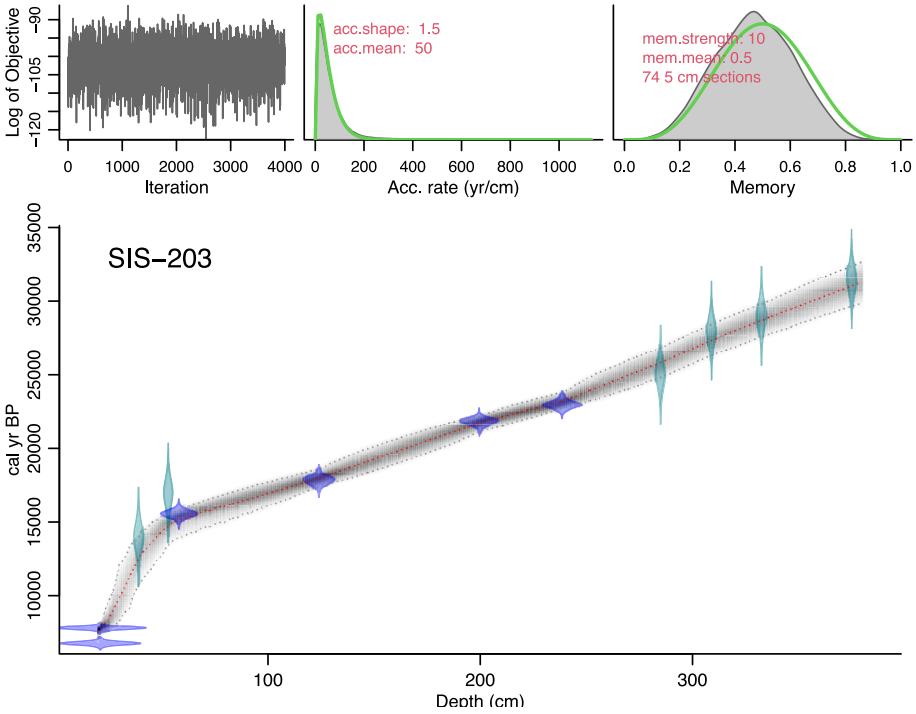

Fig. 2. Age-depth model for core SIS-203. In the bottom panel, the red stippled line shows the mean age-depth model. Confidence (at 95%) is indicated by the grey envelope. Calibrated ^{14}C dates are shown in blue and oxygen-tie points in turquoise (Table 1). Upper panels from left to right display (1) the Markov chain Monte Carlo (MCMC) iterations, the prior (green curves) and posterior (grey histograms) distributions for (2) the sedimentation rate and (3) memory.

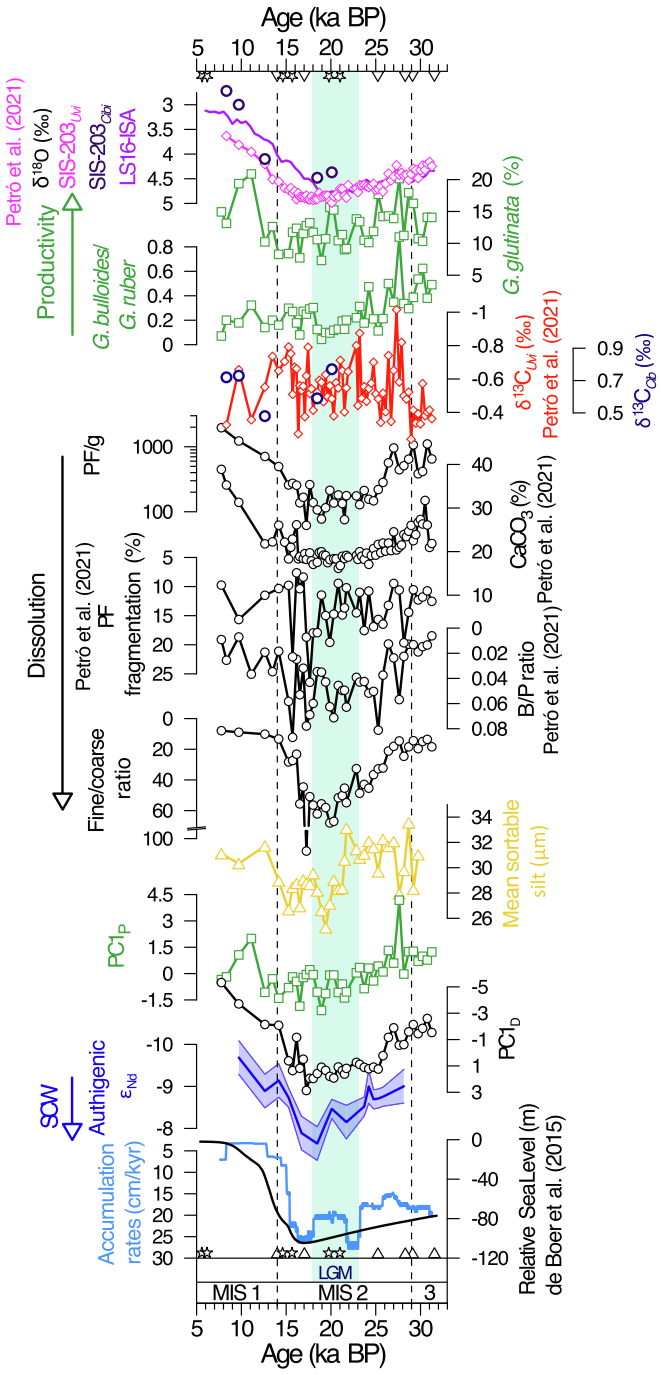

Fig. 3. Palaeoceanographic records from core SIS-203. From top to bottom: benthic foraminifera *Uvigerina* spp. (pink rhombus) and *Cibicidoides wuellerstorfi* δ^{18}O (‰, purple dots) from core SIS-203 (Petró et al., 2021 and this study, respectively) and benthic foraminifera δ^{18}O (‰, line) from LS16-ISA (Lisiecki and Stern, 2016), *G. glutinata* abundance (%, green squares), *G. bulloides/G.ruber* ratio (green squares), *Uvigerina* spp. (red rhombus) and *Cibicidoides wuellerstorfi* (purple dots) δ^{13}C (Petró et al., 2021 and this study, respectively), number of planktonic foraminifera per gram (PF/g, black dots), calcium carbonate content ($CaCO_3$, %, black dots) (Petró et al., 2021), fragmentation degree of planktonic foraminifera (%, black dots) (Petró et al., 2021), benthic and planktonic foraminifera ratio (B/P, black dots) (Petró et al., 2021), fine/coarse ratio, mean sortable silt (μm, yellow triangles), synthesised records of productivity ($PC1_P$, green squares) and dissolution ($PC1_D$, black dots), authigenic foraminiferal ε_{Nd}, accumulation rates (cm/kyr) and relative sea level (de Boer et al., 2015). Error bars in ε_{Nd} correspond to 2 standard deviations of reproducibility of the bracketing standards. Black vertical dashed lines divide the Marine Isotope Stages (MIS), and the blue band represents the Last Glacial Maximum (LGM). Stars represent ^{14}C dates and triangles the oxygen stable isotope tie-points. Palaeoproductivity proxies are shown in green while dissolution-related parameters are displayed in black. Shapes were added to the records to improve colour blindness readability.

the sediments and, where deep water is oversaturated, calcitic overgrowths can form in porewaters.

To assess the potential effect of biologically mediated dissolution, we apply a principal component analysis to synthesise the variability in primary productivity and carbonate dissolution. Our first principal component of productivity proxies ($PC1_P$) suggests an enhanced glacial productivity which can be attributed to episodic upwelling events during late MIS 3 and early MIS 2 (Fig. 3, *G. bulloides/G. ruber* ratio), in agreement with previous studies for the southern Brazilian continental margin (Alvarenga et al., 2022; Gu et al., 2018; Pereira et al., 2018;

Table 3
Oxygen ($\delta^{18}O$) and carbon ($\delta^{13}C$) stable isotopes of epibenthic foraminifera *Cibicidoides wuellerstorfi* from core SIS-203. Values reported relative to the Vienna Pee-Dee Belemnite (VPDB) standard (‰).

Depth (cm)	Age (ka BP)	$\delta^{18}O$ (‰)	$\delta^{13}C$ (‰)
25.0	8.33	2.72	0.72
29.5	9.71	3.00	0.73
39.0	12.62	4.10	0.48
133.5	18.47	4.48	0.59
166.5	20.10	4.37	0.77

Portilho-Ramos et al., 2019). A decrease in the $PC1_P$ is observed towards the deglaciation, with a slight increase during the Holocene, due to the relatively high abundance of *Globigerinita glutinata* (%).

Previous work in this region has documented biologically mediated dissolution occurring during periods of enhanced upwelling during the glacial, leading to remineralisation of organic matter at seafloor, pH decrease, and lower carbonate preservation (Suárez-Ibarra et al., 2022; 2023). However, our data suggests a different mechanism. The first principal component of carbonate dissolution ($PC1_D$) is not positively correlated with surface productivity ($PC1_P$); instead, they present a rather weak and negative (linear) correlation (Fig. 3, r = -0.35, *p*-value <0.05), which contradicts the expectation that dissolution would increase with higher productivity-driven organic flux. Rather, our results suggest that $PC1_D$ reflects other mechanisms, for instance, changes in the deep-water mass calcite saturation state. The second principal component of dissolution ($PC2_D$), which accounts for approximately 18.8% of the variance, does not show a statistically significant relationship with productivity ($PC1_P$) either. We disregard the potential for authigenic calcite overgrowths, as dissolution is the main feature documented in glacial samples and no overgrowths were observed on the foraminiferal shells during microscope observation.

Similarities between $PC1_D$ and accumulation rates (Fig. 3, r = 0.66, *p*-value <0.01) suggest a dilution effect on the carbonate content from elevated particle fluxes at our site. If vertical particle fluxes increased due to an enhanced biological pump, both elevated burial rates and decreased exposure to potentially corrosive the seafloor-water interface conditions would enhance carbonate preservation. However, both the benthic-planktonic foraminifera (B/P) ratio and the planktonic foraminifera fragmentation (PF fragmentation) index point to elevated carbonate dissolution during intervals of higher accumulation rates, suggesting that calcium carbonate was not effectively preserved by these *in situ* processes. Although sinking velocities of planktonic foraminiferal tests through the water column are relatively fast (492±295 m/day, e.g., Bach et al., 2019; Schiebel and Hemleben, 2017; Takahashi and Be, 1984), an important part of the biogenic carbonate produced at the surface ocean is dissolved before reaching the deep sea-floor (Petró et al., 2018b; Schiebel and Hemleben, 2017; Ziveri et al., 2025). This loss has been related to two mechanisms: metabolic processes and high magnesium calcites for shallow-water dissolution, and the increasing solubility of all polymorphs of $CaCO_3$ with depth for deeper waters (Sulpis et al., 2021; Berger, 1970). These observations suggest integrated water column chemistry as the primary control on carbonate preservation at our study site.

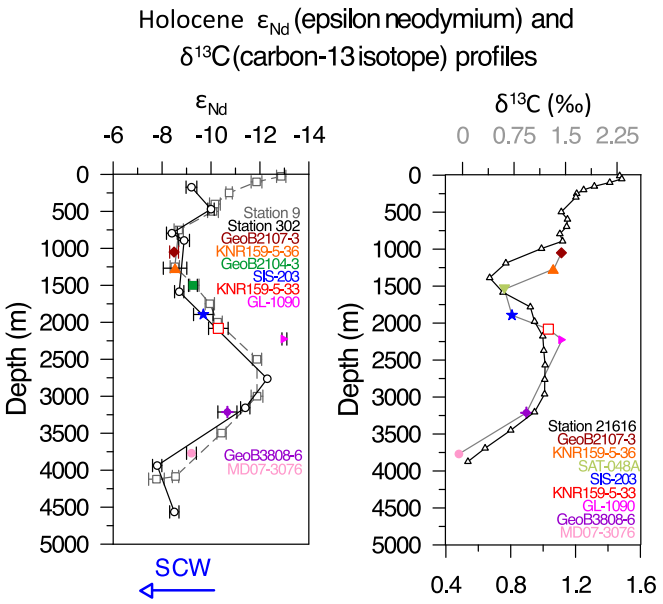

Fig. 4. Holocene neodymium isotope records (ε_{Nd}) and carbon stable isotope records ($\delta^{13}C$) from SIS-203 (this study), and nearby cores GeoB2107-3 (Howe et al., 2016b; Portilho-Ramos et al., 2018), KNR159-5-36 (Howe et al., 2016b; Oppo and Horowitz, 2000), SAT-048A (this study), GeoB2104-3 (Howe et al., 2016b; Portilho-Ramos et al., 2018), KNR159-5-33 (Howe et al., 2018), GL-1090 (Howe et al., 2016b; Lessa et al., 2017) and MD07-3076 (Gottschalk et al., 2016a; Skinner et al., 2013). ε_{Nd} analyses in GeoB3808-6 were carried out in bulk sediment (Jonkers et al., 2015). Nearby modern seawater ε_{Nd} from stations 9 (Wu et al., 2022) and SAVE station 302 (Jeandel, 1993) and $\delta^{13}C$ from station 21616 (Key et al., 2004). On the right panel, due to differences in the values scales, coretop values are plotted against the upper axis and values from station 21616 against the lower axis.

4.3. Carbonate dissolution: water mass geometry and bottom currents

Organic and inorganic dissolved carbon is redistributed within the major ocean basins by changes in the water mass circulation and stratification during different climatic states (Howe et al., 2016a; Rickaby et al., 2010). With different carbonate ion saturation levels, the relative replacement of NCW by SCW at the study site has the potential to dissolve biogenic carbonate that reaches the seafloor (Chalk et al., 2019; Oppo et al., 2023). In the Atlantic more broadly, higher proportions of SCW are generally linked to carbonate dissolution (Petró et al., 2021; Suárez-Ibarra et al., 2023), and our multi-proxy record from core SIS-203 allows us to evaluate this relationship in the western South Atlantic in detail at intermediate (ca. 1900 m) water depth.

Benthic $\delta^{13}C$ is primarily used to reconstruct water masses mixing, though can also be controlled by physical and biological processes (e.g., air-sea exchange, remineralisation) (Curry et al., 1988; Curry and Oppo, 2005; Duplessy et al., 1984, 1988; Lynch-Stieglitz et al., 1995). Our LGM

Table 4
Summary of the principal component analyses for productivity and dissolution proxies. PC means principal component, L stands for Loading (correlation with the given principal component axis), CV for cumulative variance and CE for cumulative eigen value.

		PC1			PC2			PC3			PC4		
Parameter	Proxy	L	CV	CE	L	CV	CE	L	CV	CE	L	CV	CE
Productivity	*G. bull /G. rub*	0.71	65.1	1.3	0.71	100	2.0	–	–	–	–	–	–
	G. glutinata (%)	0.71			-0.71			–			–		
	$CaCO_3$ (%)	0.47			0.26			0.33			-0.70		
	PF/g	0.49			0.22			0.01			0.65		
Dissolution	B/P	-0.5	67.8	3.30	0.22	86.6	4.30	0.83	93.8	4.60	0.19	98.3	4.90
	Fine/coarse ratio	0.51			0.14			0.24			0.18		
	PF fragmentation (%)	-0.2			0.89			-0.35			-0.03		

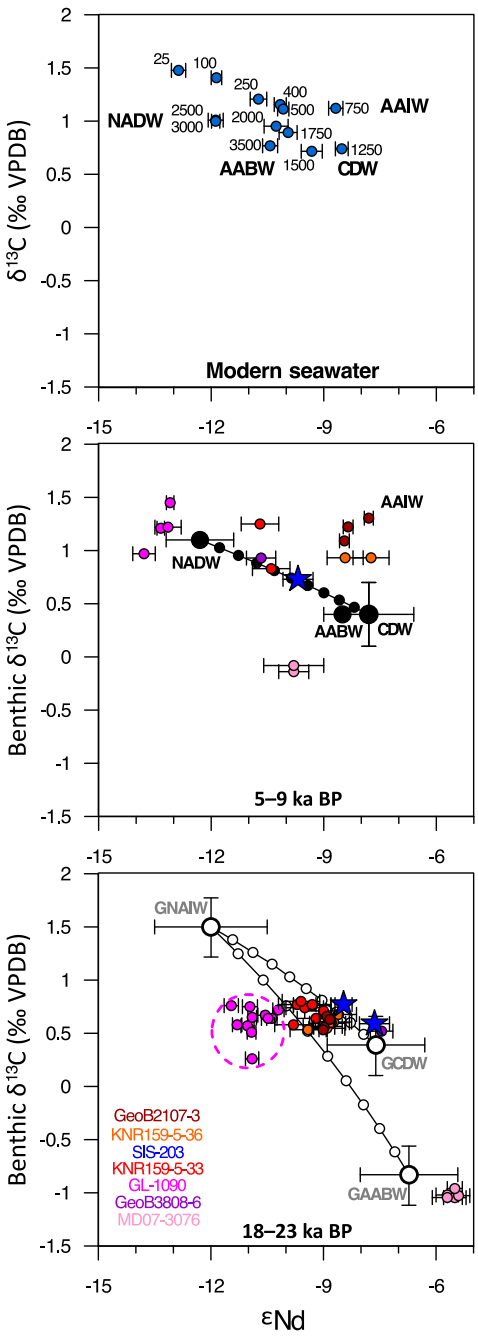

Fig. 5. Mixing model of $\delta^{13}C$ *vs.* ε_{Nd} for the study area at three different time slices. Upper panel shows modern seawater $\delta^{13}C$ from station 21616 (Key et al., 2004) and ε_{Nd} from Station 9 (Wu et al., 2022); numbers are depths in mbsl. Middle panel contains $\delta^{13}C$ and ε_{Nd} data for the 5–9 ka time interval from cores SIS-203 (this study), GeoB2107-3 (Gottschalk et al., 2016b; Portilho-Ramos et al., 2018), KNR159-5-36 (Gottschalk et al., 2016b; Oppo and Horowitz, 2000), KNR159-5-33 (Curry et al., 1988; Curry and Oppo, 2005), GL-1090 (Gottschalk et al., 2016b; Lessa et al., 2017), and MD07-3076 (Gottschalk, Vázquez Riveiros, et al. 2016; Skinner et al., 2013). ε_{Nd} analyses in GeoB3808-6 were carried out in bulk sediment (Jonkers et al., 2015). Lower panel displays $\delta^{13}C$ and ε_{Nd} data for the 18–23 ka period (Last Glacial Maximum, LGM) from the same cores as in Middle panel. The black (white) dots-line represents the binary mixing model for Holocene (LGM) NADW (GNAIW) as NCW, and AABW (GAABW) as well as CDW (GCDW) as SCW (see discussion). Some of the GL-1090 data during the LGM (pink dashed circle) might have been affected by remineralisation of organic matter which would act to reduce their $\delta^{13}C$ values.

and Holocene *Uvigerina* spp. $\delta^{13}C$ values display little variation, which alone could be attributed to the infaunal habitat of the genus *Uvigerina*, dwelling within the sediment (Zahn et al., 1986), likely influenced by pore water chemistry and/or organic matter export rather than solely bottom water mass characteristics (Hesse et al., 2014; Mackensen, 2008; Zahn et al., 1986). However, previous studies have shown that both infaunal (e.g., *Uvigerina*) and epifaunal (e.g., *Cibicidoides*) benthic foraminifera can record changes in $\delta^{13}C$ during the last deglacial (Gottschalk et al., 2016a; Skinner et al., 2013). This suggests that our $\delta^{13}C_{Uvi}$ values will partially reflect past water mass signals, in addition to changes in porewater $\delta^{13}C$. To deconvolve the multiple controls, we also use $\delta^{13}C$ from the scarce *C. wuellerstorfi* (Table 3) in the core. The LGM $\delta^{13}C_{Cib}$ values (mean 0.68±0.09) did not vary significantly with respect to Holocene $\delta^{13}C_{Cib}$ (0.72 ‰), consistent with the limited variability in $\delta^{13}C_{Uvi}$. Thus, it suggests that our benthic $\delta^{13}C_{Uvi}$ and $\delta^{13}C_{Cib}$ values do capture a rather stable carbon isotopic signature of the deep water at the site. While a broader shift in benthic $\delta^{13}C$ values from the Atlantic basin is expected due to the water masses replacement (AABW as SCW), $\delta^{13}C_{Uvi}$ and $\delta^{13}C_{Cib}$ from core SIS-203 suggest that the site is under an almost total SCW influence (in this case, glacial circumpolar deep-water, GCDW), yielding similar values for the LGM and Holocene, and consistent with reconstructions from Curry and Oppo (2005).

In contrast, $\delta^{13}C$ measurements from shallower sites in the western South Atlantic (GeoB2107-3 (Howe et al., 2016b), KNR159-5-36 (Portilho-Ramos et al., 2018)) and deeper (KNR159-5-33 (Howe et al., 2018), GL-1090 (Santos et al., 2017a, 2017b), and central South Atlantic GeoB3808-6 (Jonkers et al., 2015)) presented more positive values during the Holocene compared to core SIS-203 (Fig. 4). However, during the LGM, all these cores recorded more negative $\delta^{13}C$ values than in the Holocene, indicating a higher influence of SCW and an enhanced respired carbon storage in the mid-depth western South Atlantic during the LGM (Howe et al., 2016b; Fig. 5).

To assess the potential influence of water mass geometry changes on carbonate dynamics at our site more accurately, we reconstruct the authigenic foraminiferal ε_{Nd} from core SIS-203. Neodymium isotopes are a valuable proxy for water masses because seawater ε_{Nd} is influenced by water mass provenance and the mixing proportions, and it is not markedly fractionated by marine biological processes (Blaser et al., 2019; Frank, 2002; Piepgraas and Wasserburg, 1980; Piotrowski et al., 2008; Tachikawa et al., 2017). Furthermore, although benthic fluxes can also potentially affect ε_{Nd} under sluggish circulation, as it has been observed in other ocean basins (Du et al., 2018; Du et al., 2020), previous studies suggest that Atlantic ε_{Nd} records are a robust deep water mass tracer, even under varying circulation strengths (Howe et al., 2018; Dias et al., 2025).

The authigenic foraminiferal ε_{Nd} value from SIS-203's chronologically youngest sample (9.5±1.8 ka, ε_{Nd} = -9.69±0.04) aligns very well with modern seawater ε_{Nd} (-9.95±0.19) from nearby GEOTRACES Station 9 (Wu et al., 2022). Although measurements from the nearby Station SAVE 302 (Jeandel, 1993) are from different depths (1586 m, ε_{Nd} = -8.7±0.6; 2763 m, ε_{Nd} = -12.3±0.4), our foraminiferal ε_{Nd} values fall right in between the upper and lower points (Fig. 4). Our coretop ε_{Nd} value also corresponds closely with the Holocene authigenic foraminiferal ε_{Nd} profile, based on the immediate upper and lower sediment cores GeoB2104-3 (Howe et al., 2016b; 6.0 ka, εNd = -9.04±0.12) and KNR159-5-33 (Howe et al., 2018; εNd = 6.4 ka, εNd = -10.7±0.5), respectively. Cores GeoB3808-6 (Jonkers et al., 2015) and MD07-3076 (Skinner et al., 2013) (Fig. 4, Table 2), located in the mid-Atlantic Ridge, also align with the modern seawater and Holocene authigenic ε_{Nd} vertical profiles. The agreement between SIS-203 core top ε_{Nd} value and the seawater and nearby ε_{Nd} core tops suggests that the foraminiferal ε_{Nd} values in our study area faithfully reflect the past seawater ε_{Nd} conditions, rather than being influenced by local Nd sources (Karas et al., 2019), also suggesting that the basin is well mixed with respect to neodymium, preserving regional water masses signatures.

However, as end-member values are likely to have varied over time

(Pöppelmeier et al., 2020, 2021), converting ε_{Nd} values to proportions of ancient NCW *vs.* SCW, requires specific end-member values to be utilised (Pöppelmeier et al., 2021). Using the equation presented by Howe et al. (2016a) (see methods), we estimated NCW/SCW proportions for two intervals: Holocene (youngest sample) and Last Glacial Maximum (LGM). For the Holocene, we employ $\delta^{13}C$ and ε_{Nd} values from Pérez-Asensio et al. (2023) for the North Atlantic Deep Water (NADW), to be a pure NCW endmember, and Circumpolar Deep Water (CDW) as pure SCW endmember. The results indicate that NCW constitutes approximately 46±9% of the Holocene water mass. For the LGM, we use $\delta^{13}C$ and ε_{Nd} values from Yu et al. (2020) for the Glacial North Atlantic Intermediate Water (GNAIW, as NCW,) and $\delta^{13}C$ and ε_{Nd} values from Hu et al. (2016), Pierre et al. (2001) and Tachikawa et al. (2021) for the Glacial Circumpolar Deep Water (GCDW), as SCW. Here, LGM samples

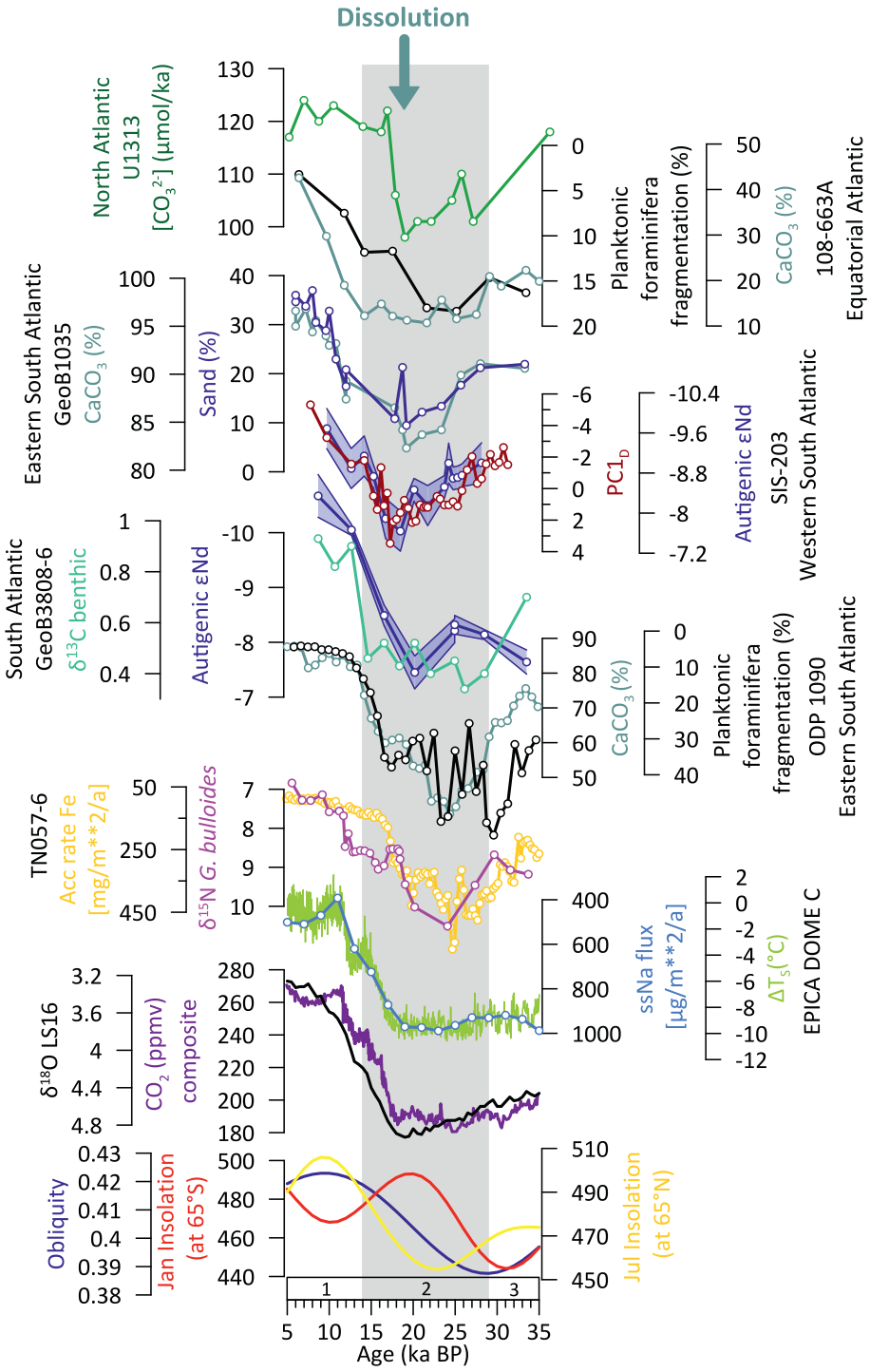

Fig. 6. Proxies for carbonate preservation from various Atlantic Ocean sediment cores and other palaeoclimatic records for the 35–5 ka BP period. The figure shows data from the North Atlantic (U1313 (Chalk et al., 2019)), Equatorial Atlantic (ODP 108-663A) and South Atlantic (GeoB1035 (Bickert and Wefer, 1996), SIS-203 (this study), GeoB3808-6 (Jonkers et al., 2015), ODP 1090 (Teitler et al., 2010)). Complementing the glacial-interglacial transition are isotopic data ($\delta^{18}O$ (Lisiecki and Stern, 2016), $\delta^{13}C$ (Jonkers et al., 2015), $\delta^{15}N$ (Martínez-García et al., 2014)), and ε_{Nd} (Jonkers et al., 2015). A widespread dissolution episode is marked with the grey vertical arrow. Temperature variations and Na fluxes from the EPICA Dome C ice core (EPICA, 2004), CO_2 composite (Bereiter et al., 2015), obliquity and insolation curves (Laskar et al., 2004) at 65°S and 65°N are included. Numbers at the bottom represent the Marine Isotope Stages.

show greater SCW relative to NCW. According to our calculations, NCW influence was reduced to approximately <13% at SIS-203 during the glacial, almost totally GCDW (Fig. 5).

Likewise, the larger SCW influence at SIS-203 during the LGM and Heinrich Stadial 1 (ca. 18.6–14.7 ka) coincides with higher $PC1_D$ values (Fig. 3). As core SIS-203 is in the interphase between SCW and NCW mixing, our multi-proxy study suggests that the carbonate preservation is predominantly impacted by water mass geometry changes. These changes likely account for a small increase in the B/P ratio (from 0 to 0.08%) and the fragmentation of planktonic foraminifera. Moreover, the replacement of NCW by SCW could also impact the carbonate preservation by lower bottom current velocities (horizontal advection), by acquiring respired CO_2 along the route to the site. This phenomenon is supported by our mean sortable silt measurements (Fig. 3), which show a decrease from the base of the core toward the LGM, suggesting a progressive reduction in bottom current strength, indicative of a more sluggish deep-water circulation (McCave et al., 2017). Whether due to geometry changes or changes in advection speed, less NCW would lead to higher amounts of respired CO_2 and a reduction in pH, and lower carbonate ion concentration, at the site causing carbonate dissolution (Howe et al., 2016a).

Carbonate dissolution records from across the Atlantic further corroborate this mechanism, pointing to a basin-wide phenomenon rather than a local specific signal (Fig. 6). Dissolution proxies from core SIS-203, GL-1090 (Dias et al., 2025) (western South Atlantic), TN057-6 (Teitler et al., 2010), ODP 1090 and GeoB1035 (Bickert and Wefer, 1996) (eastern South Atlantic), ODP 108-663A (Wagner, 2000) (equatorial Atlantic) and IODP U1313 and U1308 (Yu et al., 2016; Chalk et al., 2019) (North Atlantic) all record enhanced dissolution during the LGM. The expansion of Antarctic Bottom Water to the deep North Atlantic (Howe et al. 2016b) evidenced by more radiogenic values in authigenic ε_{Nd} (Rutberg et al., 2000; Piotrowski et al., 2008) in cores SIS-203, GeoB3808-6 (Jonkers et al., 2015) and MD07-3076 (Gottschalk et al., 2016a; Skinner et al., 2013), and of Pacific deep water to the deep South Atlantic (Williams et al., 2021) evidenced by ε_{Nd} in core MD07-3076 (Yu et al., 2020), amplified this effect by introducing carbon-enriched waters into the Atlantic basin. Biologically mediated dissolution on other sites of the southern Brazilian margin (at ~1500 m [core SAT-048A] and 2100 m [core SIS-249] depths, Suárez-Ibarra et al., 2022, 2023) and mirrored processes in eastern South Atlantic (Bickert and Wefer, 1996) indicate that both mechanisms (water mass corrosiveness and organic matter remineralisation) occurred simultaneously across the basin.

The observed shift to SCW-driven dissolution at our site is specific of "Atlantic-style" mode of carbonate preservation, now documented in the western South Atlantic. During the Mid-Pleistocene Transition (ca. 1.1 Ma), the Atlantic and Pacific Oceans diverged into anticorrelated $CaCO_3$ preservation regimes across glacial-interglacial cycles. In the "Pacific-style" regime, glacial periods show better $CaCO_3$ preservation (due to enhanced abyssal ventilation), while the Atlantic experiences heightened dissolution (Sexton and Barker, 2012; Yu et al., 2016). Our record demonstrates that the observed LGM dissolution is a regional amplification driven by the expansion of corrosive, respired carbon-rich SCW. This process emphasises the Atlantic's pivotal role *vis-a-vis* the global overturning circulation, where changes in deep-water mass geometry directly regulate carbonate preservation. Additionally, this expanded SCW included a significant component of old deep waters originating from the Pacific, which substantially increased the deep Atlantic carbon content (Yu et al., 2020). Thus, the dissolution recorded at our site provides a direct chemical record of enhanced connectivity within the glacial marine carbon cycle, whereby Southern Ocean biogeochemical changes are transmitted via deep-water masses to increase carbon storage in the Atlantic basin.

4.4. Carbon reservoir effectiveness during the Last Glacial Maximum

Understanding the physicochemical properties of the ocean during late Quaternary glacial periods is key for understanding its role as a carbon reservoir. Both, elevated primary productivity and SCW production significantly increase the deep ocean carbon storage, which in turn affects the Earth's climate system through feedback mechanisms. During glacial periods, elevated productivity enhances the flux of organic matter from the surface to the deep ocean, some of which, is effectively buried in the sediments (Cartapanis et al., 2016). This increased organic matter flux, coupled with biologically mediated dissolution, contributes to the deep ocean's role as an important carbon reservoir (Kohfeld and Chase, 2017). The remineralisation of organic matter in deep water leads to the transport and release of CO_2 to deep water masses, further enhancing carbonate dissolution.

The reduction in carbonate preservation at the study site during the LGM can be interpreted in the context of greater climatological processes (Fig. 6). During low obliquity summer solar radiation reduces (lessened seasonality), leading to cooler temperatures, less ice melt, and the buildup of polar ice (Ai et al., 2021; Paillard, 2021). This ice growth increases the Earth's albedo, creating a positive feedback loop that further cools the surface and promotes more ice formation (Berger, 1988; Petit et al., 1999). The cooling strengthens and displaces the southwesterly winds north-wards (up to 40°S), and there is evidence that this links to enhancement of iron dust-borne fertilisation of the subantarctic zone (Barkley et al., 2024; Buesseler and Andrews, 2004; Dezileau et al., 2004; Martínez-García et al., 2009, 2014; Mejía et al., 2014; Toggweiler et al., 2006; Wolff et al., 2006) and likely the southernmost Brazilian margin (Lopes et al., 2021; Suárez-Ibarra et al., 2023), which expands the biological pump (and likely carbon export) and leading to increased remineralisation of organic matter at the seafloor (Gottschalk et al., 2016b; Kohfeld et al., 2013; Martin, 1990; Roth et al., 2014). The already enhanced biological pump might have resulted in expanded organic carbon export to the seafloor by the cooler temperatures, as it has been shown that temperature affects metabolism, decreasing the remineralisation process through the water column (Boscolo-Galazzo et al., 2018), increasing the delivered organic matter, and adding to the deep-ocean carbon pool (Gottschalk et al., 2016b).

Expanded sea ice sheets may have enhanced the production of corrosive SCW during the glacial, evidenced by more radiogenic values in authigenic ε_{Nd} (Rutberg et al., 2000, Piotrowski et al., 2005) in cores SIS-203 (this study), GeoB3808-6 (Jonkers et al., 2015) and MD07-3076 (Gottschalk et al., 2016a; Skinner et al., 2013). With the addition of more organic carbon rain and associated remineralisation, SCW accumulates more respired carbon (Marzocchi and Jansen, 2019) (i.e., benthic $\delta^{13}C$ GeoB3808-6 (Jonkers et al., 2015)), becoming more undersaturated with respect to carbonate ion. The expansion of the carbon-charged SCW leads to dissolution of the exported calcareous marine plankton tests at depth.

In summary, we present a multiple proxy record from core SIS-203, which we statistically analyse to constrain the regional mechanism for glacial carbonate dissolution. The ε_{Nd} values demonstrates an almost total replacement of NCW by SCW during the LGM (Fig. 5), while sortable silt indicates a concurrent reduction in bottom current strength and thus slower deep-water ventilation speeds (Fig. 3). This sluggish circulation of an expanded SCW cell allowed for the local accumulation of respired CO_2, lowering the carbonate ion concentration ($[CO_3^{2-}]$) and pH of the bottom water at our site (Howe et al., 2016a, 2016b). The circulation change caused a reduction in the calcite saturation state (Ω calcite), and resulted in enhanced dissolution recorded by our calcium carbonate dissolution proxies (Fig. 3). The respired carbon stored in SCW may have been even larger during the LGM due to increased biological pump efficiency in the Subantarctic Zone, enhanced by iron fertilisation under strengthened southern westerly winds (Martínez-García et al., 2009). It has also been suggested that extensive Southern Ocean sea ice cover would have further promoted carbon sequestration by restricting air-sea gas exchange and strengthening SCW production (Railsback et al., 2015; Rickaby et al., 2010). Therefore, the dissolution at our study site reflects the imprint of a larger-scale glacial

reorganisation: a Southern Ocean-dominated deep sea charged with sequestered carbon, leading to effective deep-ocean carbon storage. The carbonate dissolution which we have documented in this study is controlled by water masses geometry (at ~1900 m depth, core SIS-203).

Future research, ideally utilising longer marine sediment cores, should constrain in time, space, magnitude and nature the high productive events (e.g., dust fertilisation) on the southern Brazilian continental margin, as well as their impact in carbon and carbonate burial at different sea depths.

5. Conclusion

In summary, our ε_{Nd} values demonstrates an almost total replacement of NCW by SCW during the LGM, while sortable silt indicates a reduction in bottom current strength and thus slower deep-water ventilation speeds. This study presents a refined age model for core SIS-203, revealing a significant 30 kyr offset at its base compared to previous reconstructions. While the top ages align with earlier models due to shared ^{14}C calibration, the discrepancy at the base reflects the limitations of deterministic methods like AnalySeries. The Bayesian approach (*rbacon*) accounts for sediment accumulation variability, producing a more plausible age for the base of the core (~30 ka BP vs. the previously proposed 60 ka BP). Authigenic ε_{Nd} analyses reveal a near-total Southern Component Water (SCW) influence during the Last Glacial Maximum (LGM), marked by its characteristic isotopic signature (ε_{Nd} = -7.6). This SCW expansion, combined with reduced bottom current velocities (evidenced by sortable silt mean size), likely facilitated the accumulation of respired CO_2, lowered pH, and intensified carbonate dissolution. The weak correlation ($r = -0.35$, $p > 0.05$) between productivity ($PC1_P$) and dissolution proxies ($PC1_D$) suggests that carbonate dissolution was not linked to surface productivity. Instead, this pattern further supports that dissolution was primarily driven by changes in water mass geometry rather than biologically mediated processes.

Our results identify the western South Atlantic as a key region for carbon sequestration during the LGM, with the expansion of SCW amplifying the deep ocean's capacity as an effective carbon reservoir.

CRediT authorship contribution statement

Jaime Y. Suárez-Ibarra: Writing – review & editing, Writing – original draft, Visualization, Software, Methodology, Investigation, Formal analysis, Data curation, Conceptualization. **Bruna B. Dias:** Writing – review & editing, Writing – original draft, Visualization, Software, Methodology, Investigation, Formal analysis, Data curation, Conceptualization. **Sandro M. Petró:** Writing – review & editing, Writing – original draft, Investigation, Data curation. **Cristiane F. Frozza:** Writing – review & editing, Writing – original draft, Investigation, Data curation. **Sonia Chaabane:** Writing – review & editing, Writing – original draft, Visualization, Software. **Thomas B. Chalk:** Writing – review & editing, Writing – original draft, Validation, Methodology, Formal analysis, Conceptualization. **Alexander M. Piotrowski:** Writing – review & editing, Writing – original draft, Validation, Supervision, Resources, Project administration, Methodology, Funding acquisition, Conceptualization. **Thibault de Garidel-Thoron:** Writing – review & editing, Writing – original draft, Validation, Supervision, Methodology, Conceptualization. **Maria A.G. Pivel:** Writing – review & editing, Writing – original draft, Validation, Supervision, Resources, Project administration, Methodology, Funding acquisition, Conceptualization.

Declaration of competing interest

The authors declare that they have no known competing financial interests or personal relationships that could have appeared to influence the work reported in this paper.

Acknowledgments

The authors express their gratitude to Dr. Manuel Weinkauf and the PRIMUS program (grant number PRIMUS/20/SCI/019) for sponsoring the neodymium analyses. They also acknowledge the Coordination for the Improvement of Higher Education Personnel (CAPES) for supporting the IODP Program and for financial support through Grant 88887.091727/2014-01. The authors also thank the two anonymous reviewers whose comments helped to improve the manuscript. JYSI thanks the Johanna M Resig Fellowship from the Cushman Foundation for Foraminiferal Research, the STARS and COOPERATIO program (Přírodovědecká Fakulta, Univerzita Karlova). BBD appreciates the financial support from FAPESP (grants 2018/15123-4, 2020/11452-3 and 2022/01056-9). CFF thanks the Coordination for the Improvement of Higher Education Personnel (CAPES) for her PhD scholarship. MAGP gratefully acknowledges the Brazilian National Council for Scientific and Technological Development (CNPq) for grant number 315684/2021-6. TBC and JYSI were supported through the ERC StG: 101040461.

Data availability

The ε_{Nd} dataset utilised in this study can be found at https://doi.pangaea.de/10.1594/PANGAEA.983124

References

Ai, X.E., Studer, A.S., Sigman, D.M., Martínez-García, A., Fripiat, F., Schmitt, M., Oleynik, S., Jaccard, S.L., Haug, G., 2021. Southern ocean upwelling, Earth's obliquity, and glacial-interglacial atmospheric CO2 change. Science 1348–1352.

Alvarenga, A., Paladino, I.M., Gerotto, A., DeMenocal, P., Iwai, F.S., Sousa, S.H.M., Figueira, R.C.L., Mahiques, M.M., Nagai, R.H., 2022. S/SE Brazilian continental margin sea surface temperature and productivity changes over the last 50 Kyr. Palaeogeogr. Palaeoclimatol. Palaeoecol. 601. https://doi.org/10.1016/j.palaeo.2022.111144.

Alves, E., Macario, K., Souza, R., Pimenta, A., Douka, K., Oliveira, F., Chanca, I., Angulo, R., 2015. Radiocarbon reservoir corrections on the Brazilian Coast from pre-bomb marine shells. Quat. Geochronol. 29, 30–35. https://doi.org/10.1016/j.quageo.2015.05.006.

Anderson, E.C., Libby, W.F., Weinhouse, S., Reid, A.F., Kirshenbaum, A.D., Grosse, A.V., 1947. Natural radiocarbon from cosmic radiation. Phys. Rev. 72 (10), 931–936. https://doi.org/10.1103/PhysRev.72.931.

Angulo, R.J., De Souza, M.C., Reimer, P.J., Sasaoka, S.K., 2005. Reservoir effect of the Southern and Southeastern Brazilian Coast. Radiocarbon 47 (1), 67–73. https://doi.org/10.1017/S0033822200052206.

Bach, L.T., Stange, P., Taucher, J., Achterberg, E.P., Algueró-Muñiz, M., Horn, H., Esposito, M., Riebesell, U., 2019. The influence of plankton community structure on sinking velocity and remineralization rate of marine aggregates. Glob. Biogeochem. Cycles 33 (8), 971–994. https://doi.org/10.1029/2019GB006256.

Barkley, A.E., Winckler, G., Recasens, C., Kaplan, M.R., Koffman, B.G., Calabozo, F., Middleton, J.L., Anderson, R.F., Cai, Y., Bolge, L., Longman, J., Goldstein, Steven L., 2024. Patagonian Dust, Agulhas Current, and Antarctic Ice-Rafted Debris contributions to the South Atlantic Ocean over the Past 150,000 Years. Proc. Natl. Acad. Sci. 120, 2017. https://doi.org/10.1073/pnas.

Bereiter, B., Eggleston, S., Schmitt, J., Nehrbass-Ahles, C., Stocker, T.F., Fischer, H., Kipfstuhl, S., Chappellaz, J., 2015. Revision of the EPICA Dome C CO_2 Record from 800 to 600-Kyr before Present. Geophys. Res. Lett. 42 (2), 542–549. https://doi.org/10.1002/2014GL061957.

Berger, W.H., 1970. Planktonic Foraminifera: selective solution and the lysocline. Mar. Geol. 8 (1970), 111–138.

Berger, A., 1988. Milankovitch theory and climate. Rev. Geophys. 26 (4), 624–657.

Berger, W.H., Bonneau, M.C., Parker, F.L., 1982. Foraminifera on the deep-sea floor : lysocline and dissolution rate. Oceanol. Acta 5 (2), 249–258.

Bickert, Torsten, Wefer, Gerold, 1996. Late quaternary deep water circulation in the South Atlantic: reconstruction from carbonate dissolution and benthic stable isotopes. In: 599–620 in The South Atlantic: Present and Past Circulation, edited by G. Wefer, W. H. Berger, G. Siedler, and D. Webb. Springer-Verlag, Berlin.

Blaauw, M., Christen, J.A., 2011. Flexible Paleoclimate age-depth models using an autoregressive gamma process. Bayesian Anal. 6 (3), 457–474. https://doi.org/10.1214/11-BA618.

Blaser, P., Pöppelmeier, F., Schulz, H., Gutjahr, M., Frank, M., Lippold, J., Heinrich, H., Link, J.M., Hoffmann, J., Szidat, S., Frank, N., 2019. The resilience and sensitivity of Northeast Atlantic Deep Water ε_{Nd} to overprinting by detrital fluxes over the past 30,000 years. Geochim. Cosmochim. Acta 245, 79–97. https://doi.org/10.1016/j.gca.2018.10.018.

Blaser, P., Waelbroeck, C., Thornalley, D. J.R., Lippold, J., Pöppelmeier, F., Kaboth-Bahr, S., Repschläger, J., Jaccard, S.L., 2025. Prevalent North Atlantic deep water during the Last Glacial Maximum and Heinrich Stadial 1. Nat. Geosci. https://doi.org/10.1038/s41561-025-01685-5.

Boscolo-Galazzo, F., Crichton, K.A., Barker, S., Pearson, P.N., 2018. Temperature dependency of metabolic rates in the upper ocean: a positive feedback to global climate change? Glob. Planet. Chang. 170 (March), 201–212. https://doi.org/10.1016/j.gloplacha.2018.08.017.

Broecker, W., 1982. Ocean chemistry during glacial time. Geochim. Cosmochim. Acta 46, 1689–1705. https://doi.org/10.1016/0016-7037(83)90315-0.

Brummer, G.J.A., Kucera, Michal, 2022. Taxonomic review of living planktonic foraminifera. J. Micropalaeontol. 41 (1), 29–74. https://doi.org/10.5194/jm-41-29-2022.

Buesseler, K.O., Andrews, J.E., 2004. The effects of iron fertilization. Science 304 (April), 414–417.

Cartapanis, Olivier, Bianchi, Daniele, Jaccard, Samuel L., Galbraith, Eric D., 2016. Global pulses of organic carbon burial in deep-sea sediments during glacial maxima. Nat. Commun. 7. https://doi.org/10.1038/ncomms10796.

Chalk, T.B., Foster, G.L., Wilson, P.A., 2019. Dynamic storage of glacial CO 2 in the Atlantic Ocean revealed by boron [CO 32−] and PH records. Earth Planet. Sci. Lett. 510, 1–11. https://doi.org/10.1016/j.epsl.2018.12.022.

Clark, P.U., Dyke, A.S., Shakun, J.D., Carlson, A.E., Clark, J., Wohlfarth, B., Mitrovica, J. X., Hostetler, S.W., McCabe, A.M., 2009. The Last Glacial Maximum. Science 325 (5941), 710–714. https://doi.org/10.1126/science.1172873.

Conan, S.M., Brummer, G.A., 2000. Fluxes of Planktic foraminifera in response to monsoonal upwelling on the Somalia Basin Margin. Deep-Sea Res. II 47, 2207–2227.

Conan, S.M.H., Ivanova, E.M., Brummer, G.J.A., 2002. Quantifying carbonate dissolution and calibration of foraminiferal dissolution indices in the Somali Basin. Mar. Geol. 182 (3–4), 325–349. https://doi.org/10.1016/S0025-3227(01)00238-9.

Curry, W.B., Oppo, D.W., 2005. Glacial water mass geometry and the distribution of D13C of ΣCO2 in the Western Atlantic Ocean. Paleoceanography 20, 1–13. https://doi.org/10.1029/2004PA001021.

Curry, W.B., Duplessy, J.C., Labeyrie, L.D., Shackleton, N.J., 1988. Changes in the distribution of δ13C of deep water σCO2 between the Last Glaciation and the Holocene. Paleoceanography 3 (3), 317–341.

de Boer, B., Lourens, L., Wal, R.S.W., 2015. Global 5 Million Year Sea Level, Temperature, and D18Osw Reconstructions. [Eustatic Sea Level]'. NOAA/WDS Paleoclimatology - NOAA National Centers for Environmental Information. https://doi.org/10.25921/xs31-nt56.

Dezileau, L., Ulloa, o., Hebbeln, D., Lamy, F., Reyss, J.L., Fontugne, M., 2004. Iron control of past productivity in the coastal upwelling system off the Atacama Desert, Chile. Paleoceanography 19 (3). https://doi.org/10.1029/2004PA001006.

Dias, B.B., Piotrowski, A.M., Barbosa, C.F., Venancio, I.M., Chiessi, C.M., Albuquerque, A.L.S., 2021. Coupled changes in Western South Atlantic carbon sequestration and particle reactive element cycling during millennial-scale holocene climate variability. Sci. Rep. 11 (1), 1–12. https://doi.org/10.1038/s41598-021-03821-8.

Dias, B.B., Chiessi, C.M., Piotrowski, A.M., Campos, M.C., Jena, P.S., Ballalai, J.M., Nascimento, R.A., Santos, T.P., Venancio, I.M., Mashayek, A., Albuquerque, A.L.S., 2025. Reduced penetration of northern-sourced waters into the South Atlantic during the last interglacial relative to the holocene. Paleoceanogr. Paleoclimatol. 40 (2). https://doi.org/10.1029/2024PA004955.

Du, J., Haley, B.A., Mix, A.C., Walczak, M.H., Praetorius, S.K., 2018. Flushing of the deep pacific ocean and the deglacial rise of atmospheric CO_2 concentrations. Nat. Geosci. 11 (10), 749–755. https://doi.org/10.1038/s41561-018-0205-6.

Du, J., Haley, B.A., Mix, A.C., 2020. Evolution of the global overturning circulation since the last glacial maximum based on marine authigenic neodymium isotopes. Quat. Sci. Rev. 241. https://doi.org/10.1016/j.quascirev.2020.106396.

Duplessy, J.C., Shackleton, N.J., Matthewsa, R.K., Prell, W., Ruddiman, W.F., Hendy, C. H., 1984. ^{13}C Record of Benthic Foraminifera in the Last Interglacial Ocean : Implications for the Carbon Cycle and the Global Deep Water Circulation, 243, pp. 225–243.

Duplessy, J.C., Shackleton, N.J., Fairbanks, R.G., Labeyriefi, L., Oppo, D., Labeyrie, L., Oppo, D., Kallel, N., 1988. Deepwater source variations during the last climatic cycle and their impact on the global deepwater circulation. Paleoceanography 3 (3), 343–360.

Elderfield, H., Ferretti, P., Greaves, M., Crowhurst, S., McCave, I.N., Hodell, D., Piotrowski, A.M., 2012. Evolution of ocean temperature and ice volume through the mid-pleistocene climate transition. Science 337 (6095), 704–709. https://doi.org/10.1126/science.1221294.

EPICA, 2004. Eight glacial cycles from an Antarctic Ice Core. Nature 429, 623–628. https://doi.org/10.1038/nature02599.

Frank, M., 2002. Radiogenic isotopes: tracers of past ocean circulation and Erosional Input. Rev. Geophys. 40 (1). https://doi.org/10.1029/2000RG000094, 1-1-1–38.

Frenz, M., Hoppner, R., Stuut, J.B., Wagner, T., Henrich, R., 2003. Surface sediment bulk geochemistry and grain-size composition related to the oceanic circulation along the South American Continental Margin in the Southwest Atlantic. In: Wefer, G., Mulitza, S., Ratmeyer, V. (Eds.), The South Atlantic in the Late Quaternary. Springer-Verlag, Berlin, Heidelberg, New York, Tokyo, pp. 347–373.

Frozza, C.F., Pivel, M.A.G., Suárez-Ibarra, J.Y., Ritter, M.N., Coimbra, J.C., 2020. Bioerosion on late Quaternary planktonic foraminifera related to Paleoproductivity in the Western South Atlantic. Paleoceanogr. Paleoclimatol. 35 (8), 1–16. https://doi.org/10.1029/2020PA003865.

Garcia, H.E., Locarnini, R.A., Boyer, T.P., Antonov, J.I., Baranova, O.K., Zweng, M.M., Reagan, J.R., Johnson, D.R., 2014. 'World Ocean Atlas, Volume 4: Dissolved Inorganic Nutrients (Phosphate, Nitrate, Silicate)'. Pp. 1–25 in NOAA Atlas NESDIS, edited by A. Mishonov.

Gonzales, M.V., De Almeida, F.K., Costa, K.B., Santarosa, A.C.A., Camillo J., E., de Quadros, J.P., Toledo, F.A.L., 2017. Help index: hoeglundina elegans preservation index for marine sediments in the Western South Atlantic. J. Foraminifer. Res. 47 (1), 59–69. https://doi.org/10.2113/gsjfr.47.1.56.

Gottschalk, Julia, Riveiros, Natalia Vázquez, Waelbroeck, Claire, Skinner, Luke C., Michel, Elisabeth, Duplessy, Jean Claude, Hodell, David, Mackensen, Andreas, 2016a. Carbon isotope offsets between benthic foraminifer species of the Genus Cibicides (Cibicidoides) in the Glacial Sub-Antarctic Atlantic. Paleoceanography 31 (12), 1583–1602. https://doi.org/10.1002/2016PA003029.

Gottschalk, Julia, Skinner, Luke C., Lippold, Jörg, Vogel, Hendrik, Frank, Norbert, Jaccard, Samuel L., Waelbroeck, Claire, 2016b. Biological and physical controls in the southern ocean on past millennial-scale atmospheric CO2 changes. Nat. Commun. 7 (May). https://doi.org/10.1038/ncomms11539.

Gu, F., Zonneveld, K.A.F., Chiessi, C.M., Arz, H.W., Jürgen, P., Behling, H., 2017. Long-Term Vegetation, Climate and Ocean Dynamics Inferred from a 73, 500 Years Old Marine Sediment Core (GeoB2107-3) off Southern, p. 172. https://doi.org/10.1016/j.quascirev.2017.06.028.

Gu, F., Chiessi, C.M., Zonneveld, K.A.F., Behling, H., 2018. Late quaternary environmental dynamics inferred from marine sediment core GeoB6211-2 o Ff Southern Brazil. Palaeogeogr. Palaeoclimatol. Palaeoecol. 496 (October 2017), 48–61. https://doi.org/10.1016/j.palaeo.2018.01.015.

Hammer, O., Harper, D.A.T., Ryan, P.D., 2001. Past: paleontological statistics software package for education and data analysis. Palaeontol. Electron. 4 (1), 1–9.

Hays, J.D., Imbrie, John, Shackleton, N.J., 1976. Variations in the Earth's orbit: pacemaker of the Ice Ages. Science 194 (4270), 1121–1132. https://doi.org/10.1126/science.194.4270.1121.

Heaton, Timothy J., Köhler, Peter, Butzin, Martin, Bard, Edouard, Reimer, Ron W., Austin, William E.N., Ramsey, Christopher Bronk, Grootes, Pieter M., Hughen, Konrad A., Kromer, Bernd, Reimer, Paula J., Adkins, Jess, Burke, Andrea, Cook, Mea S., Olsen, Jesper, Skinner, Luke C., 2020. Marine20 - the marine radiocarbon age calibration curve (0-55,000 Cal BP). Radiocarbon 62 (4), 779–820. https://doi.org/10.1017/RDC.2020.68.

Hesse, T., Lohmann, G., Bijma, J., Mackensen, A., Zeebe, R.E., 2014. Modelling D13C in benthic foraminifera: insights from model sensitivity experiments. Mar. Micropaleontol. 112, 50–61. https://doi.org/10.1016/j.marmicro.2014.08.001.

Howe, Jacob N.W., Piotrowski, Alexander M., Noble, Taryn L., Mulitza, Stefan, Chiessi, Cristiano M., Bayon, Germain, 2016a. North Atlantic deep water production during the Last Glacial Maximum. Nat. Commun. 7, 1–8. https://doi.org/10.1038/ncomms11765.

Howe, Jacob N.W., Piotrowski, Alexander M., Oppo, Delia W., Huang, Kuo-fang, Mulitza, Stefan, Chiessi, Cristiano M., Blusztajn, Jurek, 2016b. Antarctic intermediate water circulation in the South Atlantic over the Past 25,000 Years. Paleoceanography 31, 1302–1314. https://doi.org/10.1002/2016PA002975. Received.

Howe, Jacob N.W., Huang, Kuo-fang, Oppo, Delia W., Chiessi, Cristiano M., Mulitza, Stefan, Blusztajn, Jurek, Piotrowski, Alexander M., 2018. Similar mid-depth Atlantic water mass provenance during the Last Glacial Maximum and Heinrich Stadial 1. Earth Planet. Sci. Lett. 490, 51–61.

Hu, R., Noble, T.L., Piotrowski, A.M., McCave, I., Bostock, H.C., Neil, H.L., 2016. Neodymium isotopic evidence for linked changes in Southeast Atlantic and Southwest Pacific circulation over the last 200 Kyr. Earth Planet. Sci. Lett. 455, 106–114. https://doi.org/10.1016/j.epsl.2016.09.027.

Hua, Q., 2009. Radiocarbon: a chronological tool for the recent past. Quat. Geochronol. 4, 378–390. https://doi.org/10.1016/j.quageo.2009.03.006.

Jeandel, C., 1993. Concentration and isotopic composition of Nd in the South Atlantic Ocean. Earth Planet. Sci. Lett. 117 (3–4), 581–591. https://doi.org/10.1016/0012-821X(93)90104-H.

Jollife, I.T., Cadima, J., 2016. Principal component analysis: a review and recent developments. Philos. Transact. R. Soc. A Math. Phys. Eng. Sci. 374 (2065). https://doi.org/10.1098/rsta.2015.0202.

Jonkers, L., Zahn, R., Thomas, A., Henderson, G., Abouchami, w., François, R., Masque, P., Hall, Ian I.R., Bickert, T., 2015. Deep circulation changes in the Central South Atlantic during the Past 145 Kyrs reflected in a Combined231Pa/230Th, neodymium isotope and benthic ΔC13 record. Earth Planet. Sci. Lett. 419, 14–21. https://doi.org/10.1016/j.epsl.2015.03.004.

Karas, c., Goldstein, S.L., deMenocal, P.B., 2019. Evolution of Antarctic intermediate water during the Plio-Pleistocene and implications for global climate: evidence from the South Atlantic. Quat. Sci. Rev. 223, 1–11. https://doi.org/10.1016/j.quascirev.2019.105945.

Key, R.M., Kozyr, A., Sabine, C.L., Lee, K., Wanninkhof, R., Bullister, J.L., Feely, R.A., Millero, F.J., Mordy, C., Peng, T.H., 2004. A global ocean carbon climatology: results from global data analysis project (GLODAP). Glob. Biogeochem. Cycles 18 (4), 1–23. https://doi.org/10.1029/2004GB002247.

Kohfeld, K.E., Chase, Z., 2017. Temporal evolution of mechanisms controlling ocean carbon uptake during the Last Glacial Cycle. Earth Planet. Sci. Lett. 472, 206–215. https://doi.org/10.1016/j.epsl.2017.05.015.

Kohfeld, K.E., Graham, R.M., De Boer, A.M., Sime, L.C., Wolff, E.W., Le Quéré, C., Bopp, L., 2013. Southern Hemisphere Westerly wind changes during the Last Glacial Maximum : Paleo-data synthesis. Quat. Sci. Rev. 68, 76–95. https://doi.org/10.1016/j.quascirev.2013.01.017.

Kucera, Michal, 2007. Planktonic foraminifera as tracers of past oceanic environments. In: Pp. 213–54 in Proxies in Late Cenozoic Paleoceanography, edited by C. Hillaire-Marcel. Elsevier.

Larkin, C.S., Piotrowski, A.M., Hindshaw, R.S., Bayon, G., Hilton, R.G., Jotautas Baronas, J., Dellinger, M., Wang, R., Tipper, E.T., 2021. Constraints on the source of reactive phases in sediment from a major Arctic River using neodymium isotopes. Earth Planet. Sci. Lett. 565. https://doi.org/10.1016/j.epsl.2021.116933.

Laskar, J., Robutel, P., Joutel, F., Gastineau, M., Correia, A.C.M., Levrard, B., 2004. A long term numerical solution for the insolation quantities of the Earth. Astron. Astrophys. 428, 261–285. https://doi.org/10.1051/0004-6361:20041335.

Le, J., Shackleton, N.J., 1992. Carbonate Dissolution Fluctuations in the Western Equatorial Pacific during the Late Quaternary. Paleoceanography 7 (1), 21–42.

Lenton, T.M., Held, H., Kriegler, E., Hall, J.W., Lucht, W., Rahmstorf, S., Schellnhuber, H. J., 2008. Tipping elements in the Earth's climate system. Proc. Natl. Acad. Sci. USA 105 (6), 1786–1793. https://doi.org/10.1073/pnas.0705414105.

Lessa, D.V.O., Santos, T.P., Venancio, I.M., Albuquerque, A.L.S., 2017. Offshore expansion of the Brazilian coastal upwelling zones during marine isotope stage 5. Glob. Planet. Chang. 158 (September), 13–20. https://doi.org/10.1016/j.gloplacha.2017.09.006.

Lessa, D.V.O., Santos, T.P., Venancio, I.M., Santarosa, A.C.A., Camillo, E., Toledo, F.A.L., Costa, K.B., Albuquerque, A.L.S., 2019. Eccentricity-induced expansions of Brazilian coastal upwelling zones. Glob. Planet. Chang. 179, 33–42. https://doi.org/10.1016/j.gloplacha.2019.05.002.

Lisiecki, L.E., Raymo, M.E., 2005. A Pliocene-Pleistocene stack of 57 globally distributed benthic $\delta^{18}O$ Records. Paleoceanography 20, 1–17. https://doi.org/10.1029/2004PA001071.

Lisiecki, Lorraine E., Stern, Joseph V., 2016. Regional and global benthic $\delta^{18}O$ stacks for the last glacial cycle. Paleoceanography 31. https://doi.org/10.1002/2016PA003002 (10.1002/2016PA003002):1368–94.

Liu, X., Luo, Y., Boudreau, B.P., 2022. Effects of deep circulation on $CaCO_3$ dissolution and accumulation in the Southwestern Atlantic Ocean. Geophys. Res. Lett. 49 (2), 1–10. https://doi.org/10.1029/2021GL095020.

Locarnini, R.A., Mishonov, A.V., Antonov, J.I., Boyer, T.P., Garcia, H.E., Baranova, O.K., Zweng, M.M., Paver, C.R., Reagan, J.R., Johnson, D.R., Hamilton, M., Seidov, D., 2013. World Ocean Atlas, Volume 1: Temperature'. Pp. 1–40 in NOAA Atlas NESDIS, edited by A. Mishonov. Maryland, USA.

Lopes, R.P., Bonetti, C., Silveira dos Santos, G., Pivel, M.A.G., Petró, S.M., Caron, F., Bonetti, J., 2021. Late pleistocene sediment accumulation in the lower slope off the Rio Grande Terrace, Southern Brazilian Continental Margin. Quat. Int. 571(July 2020):97–116. https://doi.org/10.1016/j.quaint.2020.12.022.

Lynch-Stieglitz, J., Stocker, T.F., Broecker, W.S., Fairbanks, R.G., 1995. The influence of air-sea exchange on the isotopic composition of oceanic carbon. Observ. Model. 9.

Mackensen, A., 2008. On the use of benthic foraminiferal $\Delta^{13}C$ in palaeoceanography: constraints from primary proxy relationships. Geol. Soc. Lond. Spec. Publ. 303 (121–133), 121–133. https://doi.org/10.1144/SP303.9.

Mahiques, M.M., Fukumoto, M.M., Silveira, I.C.A., Figueira, R.C.L., Bícego, M.C., Lourenço, R.A., Sousa, S.H., 2007. Sedimentary changes on the Southeastern Brazilian Upper Slope during the Last 35,000 years. An. Acad. Bras. Cienc. 79 (1), 171–181.

Martin, J.H., 1990. Glacial-interglaccial CO_2 change: the iron hypothesis. Paleoceanography 5 (1), 1–13.

Martínez-García, A., Rosell-Melé, A., Geibert, W., Gersonde, R., Masqué, P., Gaspari, V., Barbante, C., 2009. Links between iron supply, marine productivity, sea surface temperature, and CO_2 over the last 1.1 Ma. Paleoceanography 24 (1), 1–14. https://doi.org/10.1029/2008PA001657.

Martínez-García, A., Sigman, D.M., Ren, H., Anderson, R.F., Straub, M., Hodell, D.A., Jaccard, S.L., Eglinton, T.I., Haug, G.H., 2014. Iron fertilization of the Subantarctic Ocean during the Last Ice Age. Science 343 (6177), 1347–1350. https://doi.org/10.1126/science.1246848.

Marzocchi, A., Jansen, M.F., 2019. Global cooling linked to increased glacial carbon storage via changes in Antarctic Sea Ice. Nat. Geosci. 12 (12), 1001–1005. https://doi.org/10.1038/s41561-019-0466-8.

McCave, I.N., Andrews, J.T., 2019. Distinguishing current effects in sediments delivered to the ocean by ice. I. Principles, methods and examples. Quat. Sci. Rev. 212, 92–107. https://doi.org/10.1016/j.quascirev.2019.03.031.

McCave, I.N., Hall, I.R., 2006. Size sorting in marine muds: processes, pitfalls, and prospects for paleoflow-speed proxies. Geochem. Geophys. Geosyst. 7 (10). https://doi.org/10.1029/2006GC001284.

McCave, I.N., Manighetti, B., Robinson, S.G., 1995. Sortable silt and fine sediment size/composition: parameters for palaeocurrent speed and palaeoceanography. Paleoceanography 10 (3), 593–610.

McCave, I.N., Thornalley, D.J.R., Hall, I.R., 2017. Relation of Sortable Silt grain-size to deep-sea current speeds: calibration of the "Mud Current Meter". Deep Sea Res. I Oceanogr. Res. Pap. 127, 1–12. https://doi.org/10.1016/j.dsr.2017.07.003.

Mejía, L.M., Ziveri, P., Cagnetti, M., Bolton, C., Zahn, R., Marino, G., Martínez-Méndez, G., Stoll, H., 2014. Effects of Midlatitude Westerlies on the Paleoproductivity at the Agulhas Bank Slope during the Penultimate Glacial Cycle: evidence from Coccolith Sr/Ca ratios. Paleoceanography 29 (7), 697–714. https://doi.org/10.1002/2013PA002589.

Milankovitch, M., 1941. Kanon Der Erdbestrahlungen Und Seine Anwendung Auf Das Eiszeitenproblem. Royal Serbian Acad. Sect. Math. Nat. Sci. 33 (Belgrade).

Nadal de Masi, M.A., 1999. Prehistoric Hunter-Gatherer Mobility on the Southern Brazilian Coast: Santa Catarina Island. Standford University.

Nguyen, T.M.P., Speijer, R.P., 2014. A new procedure to assess dissolution based on experiments on pliocene-quaternary foraminifera (ODP Leg 160, Eratosthenes Seamount, Eastern Mediterranean). Mar. Micropaleontol. 106, 22–39. https://doi.org/10.1016/j.marmicro.2013.11.004.

Oppo, D., Horowitz, M., 2000. Stable Isotope Ratios of Cibicidoides of Sediment Core KNR159-36 [Dataset]. PANGAEA.

Oppo, D.W., Lu, W., Huang, K.F., Umling, N.E., Guo, W., Yu, J., Curry, W.B., Marchitto, T.M., Wang, S., 2023. Deglacial temperature and carbonate saturation state variability in the tropical Atlantic at Antarctic intermediate water depths. Paleoceanogr. Paleoclimatol. 38 (9). https://doi.org/10.1029/2023PA004674.

Paillard, D., 2021. Climate and astronomical cycles. In: Ramstein, G. (Ed.), Paleoclimatology. Springer Nature, Switzerland.

Paillard, D., Labeyrie, L., Yiou, P., 1996. Macintosh program performs time-series analysis. EOS Trans. Am. Geophys. Union 77 (39), 379. https://doi.org/10.1029/96eo00259.

Parker, F.L., Berger, W.H., 1971. Faunal and Solution Patterns of Planktonic Foraminifera in Surface Sediments of the South Pacific. Deep-Sea Res. I 18, 73–107.

Pedrão, G.A., Hirama, M.V., Tomazella, M.O., Albuquerque, A.L.S., Chiessi, C.M., Costa, K.B., Toledo, F.A.L., 2022. Marine paleoproductivity from the last glacial maximum to the holocene in the Southwestern Atlantic: a coccolithophore assemblage and geochemical proxy perspective. Front. Earth Sci. 10 (July), 1–16. https://doi.org/10.3389/feart.2022.846245.

Pereira, L.S., Arz, H.W., Patzold, J., Portilho-Ramos, R.C., 2018. Productivity evolution in the South Brazilian bight during the last 40,000 years paleoceanography and paleoclimatology. Paleoceanogr. Paleoclimatol. 33, 1–18. https://doi.org/10.1029/2018PA003406.

Pérez-Asensio, J.N., Tachikawa, K., Vidal, L., de Garidel-Thoron, T., Sonzogni, C., Guihou, A., Deschamps, P., Jorry, S.J., Te Chen, M., 2023. Glacial expansion of carbon-rich deep waters into the southwestern indian ocean over the last 630 Kyr. Glob. Planet. Chang. 230 (October). https://doi.org/10.1016/j.gloplacha.2023.104283.

Peterson, R.G., Stramma, L., 1991. Upper-level circulation in the South Atlantic Ocean. Prog. Oceanogr. 26, 1–73.

Petit, J.R., Jouzel, J., Raynaud, D., Barkov, N.I., Barnola, J.M., Basile, I., Benders, M., Chappellaz, J., Davis, M., Delaygue, G., Delmotte, M., Kotlyakov, V.M., Legrand, M., Lipenkov, V.Y., Lorius, C., Pe, L., Ritz, C., Saltzman, E., Stievenard, M., 1999. Climate and atmospheric history of the past 420,000 years from the Vostok Ice Core, Antarctica. Nature 399, 429–436.

Petró, S.M., Burone, L., 2018. Changes in water masses in the Late Quaternary recorded at Uruguayan continental slope (south Atlantic ocean). J. Sediment. Environ. 3 (4), 280–289. https://doi.org/10.12957/jse.2018.

Petró, Sandro Monticelli, da Costa, Elisa, Oliveira, María Pivel, Alejandra, Gómez, Coimbra, João Carlos, 2018a. Registro Das Flutuações Da Lisoclina e Da CCD No Quaternário Tardio Na Bacia de Pelotas. Anuário Do Instituto de Geociências - UFRJ 41 (2), 710–719.

Petro, S.M., Ritter, M.D.N., Pivel, M.A.G., Coimbra, J.C., 2018b. Surviving in the water column: defining the taphonomically active zone in pelagic systems. Palaios 33, 85–93. https://doi.org/10.2110/palo.2017.032.

Petró, S.M., Pivel, M.A.G., Coimbra, J.C., 2021. Evidence of supra-lysoclinal dissolution of pelagic calcium carbonate in the Late Quaternary in the Western South Atlantic. Mar. Micropaleontol. 166 (December 2020). https://doi.org/10.1016/j.marmicro.2021.102013.

Piepgraas, D.J., Wasserburg, G.J., 1980. Neodymium isotopic variations in seawater. Earth Planet. Sci. Lett. 50, 128–138. https://doi.org/10.1016/j.gca.2018.10.018.

Pierre, C., Saliège, J.F., Urrutiaguer, M.J., Giraudeau, J., 2001. Stable Isotope Record of Benthic and Planktonic Foraminifera from ODP Site 175-1087 in the Southern Cape Basin, Atlantic Ocean [Dataset Publication Series]. PANGAEA.

Piola, A.R., Matano, R.P., 2019. Ocean currents: atlantic western boundary—Brazil current/Falkland (Malvinas) current. Re. Module Earth Sys. Environ. Sci. 3 (December), 414–420. https://doi.org/10.1016/b978-0-12-409548-9.10541-x.

Piotrowski, A.M., Goldstein, S.L., Hemming, S.R., Fairbanks, R.G., 2005. Temporal relationships of carbon cycling and ocean circulation at glacial boundaries. Science 307, 1933–1938. https://doi.org/10.1126/science.1104883.

Piotrowski, A.M., Goldstein, S.L., Sidney, R.H., Fairbanks, R.G., Zylberberg, D.R., 2008. Oscillating glacial northern and southern deep water formation from combined neodymium and carbon isotopes. Earth Planet. Sci. Lett. 272 (1–2), 394–405. https://doi.org/10.1016/j.epsl.2008.05.011.

Pöppelmeier, F., Gutjahr, M., Blaser, P., Oppo, D.W., Jaccard, S.L., Regelous, M., Huang, K.F., Süfke, F., Lippold, J., 2020. Water mass gradients of the mid-depth southwest atlantic during the Past 25,000 years. Earth Planet. Sci. Lett. 531. https://doi.org/10.1016/j.epsl.2019.115963.

Pöppelmeier, F., Gutjahr, M., Blaser, P., Schulz, H., Süfke, F., Lippold, J., 2021. Stable Atlantic deep water mass sourcing on glacial-interglacial timescales. Geophys. Res. Lett. 48 (15), 1–10. https://doi.org/10.1029/2021GL092722.

Pöppelmeier, F., Lippold, J., Blaser, P., Gutjahr, M., Frank, M., Stocker, T.F., 2022. Neodymium isotopes as a paleo-water mass tracer: a model-data reassessment. Quat. Sci. Rev. 279. https://doi.org/10.1016/j.quascirev.2022.107404.

Portilho-Ramos, R.C., Cruz, A.P.S., Barbosa, C.F., Rathburn, A.E., Mulitza, S., Venancio, I.M., Tilmann Schwenk, C., Rühlemann, Vidal, L., Chiessi, C.M., Silveira, C.S., 2018. Methane release from the Southern Brazilian Margin during the Last Glacial. Sci. Rep. 8 (5948), 50–55. https://doi.org/10.1038/s41598-018-24420-0.

Portilho-Ramos, R.C., Pinho, M.T.L., Chiessi, C.M., Barbosa, C.F., 2019. Understanding the mechanisms behind high glacial productivity in the Southern Brazilian Margin. Clim. Past 15, 943–955. https://doi.org/10.5194/cp-15-943-2019.

Railsback, L. Bruce, Gibbard, Philip L., Head, Martin J., Ny, Riavo G., Voarintsoa, and Samuel Toucanne., 2015. An optimized scheme of lettered marine isotope substages for the last 1.0 million years, and the climatostratigraphic nature of isotope stages and substages. Quat. Sci. Rev. 111, 94–106. https://doi.org/10.1016/j.quascirev.2015.01.012.

Rickaby, R.E.M., Elderfield, H., Roberts, N., Hillenbrand, C.D., Mackensen, A., 2010. Evidence for elevated alkalinity in the glacial Southern Ocean. Paleoceanography 25 (1), 1–15. https://doi.org/10.1029/2009PA001762.

Roberts, N.L., Piotrowski, A.M., Elderfield, H., Eglinton, T.I., Lomas, M.W., 2012. Rare earth element association with foraminifera. Geochim. Cosmochim. Acta 94, 57–71. https://doi.org/10.1016/j.gca.2012.07.009.

Robinson, S., Ivanovic, R.F., Gregoire, L.J., Tindall, J., Van De Flierdt, T., Plancherel, Y., Pöppelmeier, F., Tachikawa, K., Valdes, P.J., 2023. Simulating marine neodymium isotope distributions using Nd v1.0 coupled to the ocean component of the FAMOUS-MOSES1 climate model: sensitivities to reversible scavenging efficiency and benthic source distributions. Geosci. Model Dev. 16 (4), 1231–1264. https://doi.org/10.5194/gmd-16-1231-2023.

Roth, R., Ritz, S.P., Joos, F., 2014. Burial-nutrient feedbacks amplify the sensitivity of atmospheric carbon dioxide to changes in organic matter remineralisation. Earth Syst. Dynam. 5 (2), 321–343. https://doi.org/10.5194/esd-5-321-2014.

Rutberg, R.L., Hemming, S.R., Goldstein, S.L., 2000. Reduced North Atlantic deep water flux to the glacial Southern Ocean inferred from neodymium isotope ratios. Nature 405 (6789), 935–938. https://doi.org/10.1038/35016049.

Santos, Thiago P., Lessa, Douglas O., Venancio, Igor M., Chiessi, Cristiano M., Mulitza, Stefan, Kuhnert, Henning, Govin, Aline, Machado, Thiago, Costa, Karen B., Toledo, Felipe, Dias, Bruna B., Luiza, Ana, Albuquerque, S., 2017a. Prolonged warming of the brazil current precedes deglaciations prolonged warming of the brazil current precedes deglaciations. Earth Planet. Sci. Lett. 463 (April), 1–12. https://doi.org/10.1016/j.epsl.2017.01.014.

Santos, Thiago P., Lessa, Douglas V.O., Venancio, Igor Martins, Chiessi, Cristiano Mazur, Mulitza, Stefan, Kuhnert, H., et al., 2017b. Stable oxygen isotope record during termination II in sediment core GL1090. PANGAEA. https://doi.org/10.1594/PANGAEA.884583.

Schiebel, R., Hemleben, C., 2017. Planktic Foraminifers in the Modern Ocean: Ecology, Biogeochemistry, and Application.

Schlitzer, Reiner, 2023. Ocean Data View. https://odv.awi.de.

Sexton, P.F., Barker, S., 2012. Onset of "Pacific-Style" deep-sea sedimentary carbonate cycles at the mid-pleistocene transition. Earth Planet. Sci. Lett. 321–322, 81–94. https://doi.org/10.1016/j.epsl.2011.12.043.

Shackleton, N.J., 2000. The 100, 000-year ice-age cycle identified and found to lag temperature, carbon dioxide, and orbital eccentricity, 289 (September), 1897–1902.

Shub, A.B., Lund, D.C., Oppo, D.W., Garity, M.L., 2024. Brazil margin stable isotope profiles for the last glacial cycle: implications for watermass geometry and oceanic carbon storage. Paleoceanogr. Paleoclimatol. 39 (1). https://doi.org/10.1029/2023PA004635.

Sigman, D.M., Boyle, E.A., 2000. Glacial/interglacial changes in atmospheric carbon dioxide. Nature 407 (October), 859–869.

Skinner, L.C., Scrivner, A.E., Vance, D., Barker, S., Fallon, S., Waelbroeck, C., 2013. North Atlantic versus Southern Ocean contributions to a deglacial surge in deep ocean ventilation. Geology 41 (6), 667–670. https://doi.org/10.1130/G34133.1.

Steinsund, P.I., Hald, M., 1994. Recent calcium carbonate dissolution in the barents sea: paleoceanographic applications. Mar. Geol. 117 (1–4), 303–316. https://doi.org/10.1016/0025-3227(94)90022-1.

Stuiver, Minze, Reimer, Paula J., 1993. Extended ^{14}C data base and revised CALIB 3.0 ^{14}C age calibration program. Radiocarbon 35 (1), 215–230. https://doi.org/10.1017/S0033822200013904.

Suárez-Ibarra, J.Y., Frozza, C.F., Petró, S.M., Pivel, M.A.G., 2021. Fragment or broken? Improving the planktonic foraminifera fragmentation assessment. Palaios 36 (5), 165–172. https://doi.org/10.2110/palo.2020.062.

Suárez-Ibarra, J.Y., Frozza, C.F., Palhano, P.L., Petró, S.M., Weinkauf, M.F.G., Pivel, M.A.G., 2022. Calcium carbonate dissolution triggered by high productivity during the last glacial–interglacial interval in the deep Western South Atlantic'. Front. Earth Sci. 10 (March), 1–14. https://doi.org/10.3389/feart.2022.830984.

Suárez-Ibarra, Jaime Yesid, Freire, Tiago Menezes, Frozza, Cristiane Fraga, Pinho, Tainã M.L., Petró, Sandro Monticelli, Dias, Bruna B., Chalk, Thomas B., Chaabane, Sonia, Srivastava, Medhavi, Costa, Karen Badaraco, Toledo, Felipe A.L., de Garidel-Thoron, Thibault, Coimbra, João Carlos, Pivel, María Alejandra Gómez, 2023. Surface fertilisation and organic matter delivery enhanced carbonate dissolution in the Western South Atlantic. Front. Ecol. Evol. 11 (1238334), 1–14. https://doi.org/10.3389/fevo.2023.1238334.

Sulpis, O., Jeansson, E., Dinauer, A., Lauvset, S.K., Middelburg, J.J., 2021. Calcium carbonate dissolution patterns in the ocean. Nat. Geosci. 14 (6), 423–428. https://doi.org/10.1038/s41561-021-00743-y.

Tachikawa, K., Arsouze, T., Bayon, G., Bory, A., Colin, C., Dutay, J.C., Frank, N., Giraud, X., Gourlan, A.T., Jeandel, C., Lacan, F., Meynadier, L., Montagna, P., Piotrowski, A.M., Plancherel, Y., Pucéat, E., Roy-Barman, M., Waelbroeck, C., 2017. The large-scale evolution of neodymium isotopic composition in the global modern and Holocene ocean revealed from seawater and archive data. Chem. Geol. 457 (December 2016), 131–148. https://doi.org/10.1016/j.chemgeo.2017.03.018.

Tachikawa, K., Rapuc, W., Vidal, L., Dubois-Dauphin, Q., Westerhold, T., Guihou, A., Bickert, T., Pérez-Asensio, J., Deschamps, P., Skonieczny, C., 2021. Eastern atlantic deep-water circulation and carbon storage inferred from neodymium and carbon isotopic compositions over the past 1.1 million years. Quat. Sci. Rev. 252 (106752). https://doi.org/10.1016/j.quascirev.2020.106752ï.

Takahashi, K., Be, A.W.H., 1984. Planktonic foraminifera: factors controlling sinking speeds. Deep Sea Res. Part A 31 (12), 1477–1500. https://doi.org/10.1016/0198-0149(84)90083-9.

Tanaka, T., Togashi, S., Kamioka, H., Amakawa, H., Kagami, H., Hamamoto, T., Yuhara, M., Orihashi, Y., Yoneda, S., Shimizu, H., Kunimaru, T., Takahashi, K., Yanagi, T., Nakano, T., Fujimaki, H., Shinjo, R., Asahara, Y., Tanimizu, M., Dragusanu, C., 2000. JNdi-1: A Neodymium Isotopic Reference in Consistency with LaJolla Neodymium. Chem. Geol. 168 (3–4), 279–281. https://doi.org/10.1016/S0009-2541(00)00198-4.

Teitler, L., Warnke, D.A., Venz, K.A., Hodell, D.A., Becquey, S., Gersonde, R., Teitler, W., 2010. Determination of Antarctic ice sheet stability over the last ~500 Ka through a study of iceberg-rafted debris. Paleoceanography 25 (1), 1–18. https://doi.org/10.1029/2008PA001691.

Toggweiler, J.R., Russell, J.L., Carson, S.R., 2006. Midlatitude westerlies, atmospheric CO2, and climate change during the ice ages. Paleoceanography 21, 1–15. https://doi.org/10.1029/2005PA001154.

Wagner, T., 2000. Control of organic carbon accumulation in the late quaternary equatorial atlantic (ocean drilling program sites 664 and 663): productivity versus terrigenous supply. Paleoceanography 15 (2), 181–199. https://doi.org/10.1029/1999PA000406.

Williams, T.J., Martin, E.E., Sikes, E., Starr, A., Umling, N.E., Glaubke, R., 2021. Neodymium isotope evidence for coupled southern ocean circulation and antarctic climate throughout the Last 118,000 years. Quat. Sci. Rev. 260. https://doi.org/10.1016/j.quascirev.2021.106915.

Wolff, E.W., Fischer, H., Fundel, F., Ruth, U., Twarloh, B., Littot, G.C., Mulvaney, R., Röthlisberger, R., De Angelis, M., Boutron, C.F., Hansson, M., Jonsell, U., Hutterli, M.A., Lambert, F., Kaufmann, P., Stauffer, B., Stocker, T.F., Steffensen, J.P., Bigler, M., Siggaard-Andersen, M.L., Udisti, R., Becagli, S., Castellano, E., Severi, M., Wagenbach, D., Barbante, C., Gabrielli, P., Gaspari, V., 2006. Southern ocean sea-ice extent, productivity and iron flux over the past eight glacial cycles. Nature 440 (7083), 491–496. https://doi.org/10.1038/nature04614.

Wu, Y., Pena, L.D., Anderson, R.F., Hartman, A.E., Bolge, L.L., Basak, C., Kim, J., Rijkenberg, M.J.A., de Baar, H.J.W., Goldstein, S.L., 2022. Assessing neodymium isotopes as an ocean circulation tracer in the Southwest Atlantic. Earth Planet. Sci. Lett. 599, 117846. https://doi.org/10.1016/j.epsl.2022.117846.

Yehudai, M., Tweed, L.E., Ridge, S., Yingzhe, W., Goldstein, S.L., 2023. Effects of past Nd seawater concentrations on Nd-isotope Paleocirculation reconstructions: a Bayesian approach. Geophys. Res. Lett. 50 (21). https://doi.org/10.1029/2023GL104489.

Yu, J., Menviel, L., Jin, Z.D., Thornalley, D.J.R., Barker, S., Marino, G., Rohling, E.J., Cai, Y., Zhang, F., Wang, X., Dai, Y., Chen, P., Broecker, W.S., 2016. Sequestration of carbon in the deep Atlantic during the Last Glaciation. Nat. Geosci. 9 (4), 319–324. https://doi.org/10.1038/ngeo2657.

Yu, J., Menviel, L., Jin, Z.D., Anderson, R.F., Jian, Z., Piotrowski, A.M., Ma, X., Rohling, E.J., Zhang, F., Marino, G., McManus, J.F., 2020. Last glacial atmospheric CO2 decline due to widespread pacific deep-water expansion. Nat. Geosci. 13 (9), 628–633. https://doi.org/10.1038/s41561-020-0610-5.

Zahn, R., Winn, K., Sarnthein, M., 1986. Benthic foraminiferal Δ^{13}C and accumulation rates of organic carbon *Uvigerina Peregrina* group and *Cibicidoides wuellerstorfi*. Paleoceanography 1 (1), 27–42.

Ziveri, P., Langer, G., Chaabane, S., de Vries, J., Gray, W.R., Keul, N., Hatton, I.A., Manno, C., Norris, R., Pallacks, S., Young, J.R., Schiebel, R., Zarkogiannis, S., Anglada-Ortiz, G., Bianco, S., de Garidel-Thoron, T., Grelaud, M., Lucas, A., Probert, I., Mortyn, P.G., 2025. Calcifying Plankton: from biomineralization to global change. Science 390 (6771).